

SUPPORTING INFORMATION

ESR analyses of picket fence Mn^{II} and 6th ligand coordinated Fe^{III} porphyrins ($S = 5/2$) and a Co^{II}(*hfac*) complex ($S = 3/2$) with sizable ZFS parameters revisited: A full spin Hamiltonian approach and quantum chemical calculations

Takeshi Yamane,¹ Kenji Sugisaki,¹ Hideto Matsuoka,¹ Kazunobu Sato,^{*1} Kazuo Toyota,¹ Daisuke Shiomi,¹ and Takeji Takui^{*1,2}

¹Department of Chemistry and Molecular Materials Science, Graduate School of Science, Osaka City University, 3-3-138, Sugimoto, Sumiyoshi, Osaka 558-8585, Japan

²Support Department/University Research Administrator Center, University Administration Division, Osaka City University, 3-3-138, Sugimoto, Sumiyoshi, Osaka 558-8585, Japan

Contents

1. Derivation of the analytical expressions for the $g^{\text{eff}}/g^{\text{true}}$ relationships in the case of the non-collinearity between the g - and rank-2 ZFS tensors for the spin quantum number $S = 3/2$ and $5/2$: The exact analytical expressions and genuine Zeeman perturbation based analytical formulas.

Figure S1. Energy diagram of the spin states, denoted by M_S , based on both the exact solution and the genuine Zeeman perturbation approaches for the non-collinear case with the static magnetic field \mathbf{B} parallel to the principal z -axis of the ZFS tensor.

2. Analyses of the X-band fine-structure/hyperfine structure ESR spectra of complexes 1–3 revisited

(a) [Mn(TpivPP)X] (complex 1, X = 1-MeIm; complex 2, X = 2-MeHIm)

Table S1. The experimental g -values of complexes **1** and **2**, as revisited and reanalyzed in this work in terms of the fictitious spin-1/2 and full spin Hamiltonian approaches to their X-band ESR spectra: The microwave frequency of 9.45 (three significant digits) GHz was taken from the reported paper.

Figure S2. The simulated X-band (9.45 GHz) ESR spectra of [Mn^{II}(TpivPP)(1-MeIm)] (complex **1**) in powder at 90 K based on both the fictitious spin-1/2 Hamiltonian and the true spin Hamiltonian which includes the rank-2 ZFS tensor.

Figure S3. (a) The energy diagrams of complex **1** for the principal axis orientations as a function of the magnitude of the static magnetic field and (b) the angular dependence of the resonance fields for complex **1** from the principal z - to y -axis, based on the true spin Hamiltonian approach.

Figure S4. The simulated X-band (9.45 GHz) ESR spectra of [Mn^{II}(TpivPP)(2-MeHIm)] (complex **2**) in powder at 90 K based on both the fictitious spin-1/2 Hamiltonian and true spin Hamiltonian including the rank-2 ZFS tensor.

Figure S5 (a) The energy diagrams of complex **2** for the principal axis orientations as a function of the magnitude of the static magnetic field and (b) the angular dependence of the resonance fields for complex **2** from the principal z - to y -axis, based on the full spin Hamiltonian approach.

Table S2. The experimental principal values and E/D of the experimental magnetic tensors of manganese complexes **1** and **2**, as determined in terms of the full spin Hamiltonian approach.

Table S3. The theoretical principal values and E/D of the magnetic tensors of manganese complexes **1** and **2**, as obtained by the quantum chemical calculations on the basis of the NOB-PK method at the UBP86/Sapporo-DZP, 3-21g level.

Figure S6. (a) The theoretical X-band (9.45 GHz) ESR spectrum of **1** in powder at 90 K based on the full spin Hamiltonian which includes the rank-2 ZFS tensor. (b) The angular dependence of the ESR spectra in only the three principal axis planes for clarity.

Figure S7. (a) The theoretical X-band (9.45 GHz) ESR spectrum of **2** in powder at 90 K based on the full spin Hamiltonian which includes the rank-2 ZFS tensor. The spin Hamiltonian parameters are based on the theoretical ones, and the magnetic tensors are assumed to be collinear. (b) The angular dependence of the ESR spectra in only the three principal axis planes for clarity.

Figure S8. The ratio of $g^{\text{eff}}/g^{\text{true}}$ as a function of E/D for the $|M_S = 1/2\rangle$ -dominant transition, as calculated by using the exact solution of the rank-2 ZFS + Zeeman interaction Hamiltonian for $h\nu/D = 9.45 \text{ GHz}/20 \text{ GHz} = 0.47$ with $S = 5/2$ in the case of the collinearity between the g - and ZFS tensors.

(b) [FeTPP(4-PyNO)]BF₄, **3**·BF₄: Complex **3**

Table S4. The theoretical principal values and E/D of the magnetic tensors of complex **3**⁺, as obtained by the quantum chemical calculations on the basis of the NOB-PK method at the UBP86/Sapporo-DZP, 3-21g level.

Table S5. Comparison of the D^{SO} tensor contribution between the NOB-PK and PK methods for complexes **1–3**.

Analysis of the SQUID Data of complex **3** revisited.

Figure S9. The calculated temperature dependence of the effective magnetic moments (μ_{eff}) for (a) the solution and (b) micro-crystalline samples of **3**·BF₄.

Figure S10. The simulated spectrum of complex **3**⁺ based on the reported fictitious spin-1/2 magnetic tensors and the simulated one based on the ZFS + electronic Zeeman interaction Hamiltonian approach.

Figure S11. The simulated spectrum of complex **3**⁺ based on the reported fictitious spin-1/2 magnetic tensors and the simulated one based on the theoretical magnetic tensor.

Figure S12. The energy diagrams calculated for **3**⁺ ($S = 5/2$) in the case of the static magnetic field parallel to (a) the principal x -axis and (b) the principal y -axis (X-band).

Figure S13. The simulated Q-band ESR spectrum of complex **3** based on the reported magnetic tensors and the theoretical magnetic tensors.

Figure S14. The energy diagrams calculated for **3**⁺, ($S = 5/2$) in the case of the static magnetic field parallel to (a) the principal x -axis and (b) the principal y -axis (Q-band).

Figure S15. The simulated angular dependence of ESR spectra of **3**⁺ by using of the calculated magnetic parameters.

Figure S16. The simulated W-band ESR spectrum of **3**⁺ based on the reported magnetic tensors and the theoretical magnetic tensors.

Figure S17. The energy diagrams of **3**⁺ calculated with the static magnetic field oriented parallel to the principal axes.

Figure S18. The simulated angular dependence of ESR spectra of **3**⁺ by using of the calculated magnetic parameters.

(c) *cis*-[Co^{II}(hfac)₂(H₂O)₂], complex 4

Figure S19. The ESR spectra of complex **4** obtained from the fictitious spin-1/2 and full spin Hamiltonians with (a) $E/D =$ (a) 0.05, (b) 0.1, (c) 0.15, (d) 0.2 (e) 0.25 and (f) 0.3.

Table S6. The sets of spin Hamiltonian parameters obtained from the spectral simulation. The g -values are given as optimized as a function of E/D .

Figure S20. The plot of $g^{\text{eff}}/g^{\text{true}}$ shown in Table S6.

Figure S21. The simulated (a) magnetization curve and (b) magnetic susceptibility of complex **4**.

Non-collinear case

Figure S22. The simulated randomly-oriented (powder-pattern) ESR spectra of **4** magnetically diluted in diamagnetic *cis*-[Zn(hfac)₂(H₂O)₂].

Figure S23. The relationships of the g^{eff} and g^{true} -values, as calculated in terms of the exact eigen-energy/-value approach in the non-collinear case.

1. Derivation of the analytical expressions for the $g^{\text{eff}}/g^{\text{true}}$ relationships in the case of the non-collinearity between the g - and rank-2 ZFS tensors for the spin quantum number $S = 3/2$ and $5/2$: The exact analytical expressions and genuine Zeeman perturbation based analytical formulas.

In this work, we have given the analytical expressions below for only $S = 3/2$ and $5/2$, and the generalization to the non-collinear cases, as presented here, are extended to higher spin multiplicities, particularly by invoking the genuine Zeeman perturbation treatment.

The principal axis coordinate system (x, y, z) is taken as that of the rank-2 ZFS tensor. Introducing the direction cosines, $\cos \theta_{ij'}$'s, which define the relative orientation of the non-collinear g -tensor with respect to the ZFS \mathbf{D} -tensor. $\theta_{ij'}$ ($i = x, y, z; j' = x', y', z'$) is an angle between the i -axis of the \mathbf{D} -tensor and the j' -axis of the \mathbf{g}' -tensor. Thus, a transformation matrix U is given as

$$U = \begin{pmatrix} \cos \theta_{xx'} & \cos \theta_{xy'} & \cos \theta_{xz'} \\ \cos \theta_{yx'} & \cos \theta_{yy'} & \cos \theta_{yz'} \\ \cos \theta_{zx'} & \cos \theta_{zy'} & \cos \theta_{zz'} \end{pmatrix}$$

The \mathbf{g}' -tensor is given in its original principal coordinate axis system (x', y', z') as

$$\mathbf{g}' = \begin{pmatrix} g_{x'} & 0 & 0 \\ 0 & g_{y'} & 0 \\ 0 & 0 & g_{z'} \end{pmatrix}$$

The matrix U transforms \mathbf{g}' into \mathbf{g} in terms of the principal coordinate axis system (x, y, z) as

$$\mathbf{g} = U\mathbf{g}'U^T = \begin{pmatrix} \cos \theta_{xx'} & \cos \theta_{xy'} & \cos \theta_{xz'} \\ \cos \theta_{yx'} & \cos \theta_{yy'} & \cos \theta_{yz'} \\ \cos \theta_{zx'} & \cos \theta_{zy'} & \cos \theta_{zz'} \end{pmatrix} \begin{pmatrix} g_{x'} & 0 & 0 \\ 0 & g_{y'} & 0 \\ 0 & 0 & g_{z'} \end{pmatrix} \begin{pmatrix} \cos \theta_{xx'} & \cos \theta_{yx'} & \cos \theta_{zx'} \\ \cos \theta_{xy'} & \cos \theta_{yy'} & \cos \theta_{zy'} \\ \cos \theta_{xz'} & \cos \theta_{yz'} & \cos \theta_{zz'} \end{pmatrix}$$

where U^T denotes the transposed matrix of U . The rank-2 ZFS and electronic Zeeman interaction Hamiltonian is given in the principal axis coordinate system as

$$H = \mathbf{S} \cdot \mathbf{D} \cdot \mathbf{S} + \beta \mathbf{S} \cdot \mathbf{g} \cdot \mathbf{B}$$

When the static magnetic field is oriented along the z -axis, i.e., with $\mathbf{B} = \begin{pmatrix} 0 \\ 0 \\ B \end{pmatrix}$, H is given as

$$H = D \left[S_z^2 - \frac{1}{3} S(S+1) \right] + E(S_x^2 - S_y^2) + (S_x g_{xz'} + S_y g_{yz'} + S_z g_{zz'}) \beta B$$

where $g_{ij'}$ denotes the ij' component of the \mathbf{g} -tensor in terms of the principal axis coordinate system (x, y, z) , defined as

$$\begin{aligned} g_{xz'} &= g'_{xz} = g_{x'} \cos \theta_{xx'} \cos \theta_{zx'} + g_{y'} \cos \theta_{xy'} \cos \theta_{zy'} + g_{z'} \cos \theta_{xz'} \cos \theta_{zz'} \\ g_{yz'} &= g'_{yz} = g_{x'} \cos \theta_{yx'} \cos \theta_{zx'} + g_{y'} \cos \theta_{yy'} \cos \theta_{zy'} + g_{z'} \cos \theta_{yz'} \cos \theta_{zz'} \\ g_{zz'} &= g'_{zz} = g_{x'} \cos^2 \theta_{zx'} + g_{y'} \cos^2 \theta_{zy'} + g_{z'} \cos^2 \theta_{zz'} \end{aligned}$$

Since there is no confusion as to the definition of the principal axis coordinates, we introduce g'_{ij} instead of $g_{ij'}$ for simplicity. Throughout the derivation below, the prime of g'_{ij} is kept so as to represent the non-collinearity of the \mathbf{g} -tensor.

1.1 Spin-quartet state ($S = 3/2$)

The matrix representation of the rank-2 ZFS tensor + electronic Zeeman interaction Hamiltonian for $S = 3/2$ is given in the $|M_S\rangle$ basis set as

$$\begin{pmatrix} D + \frac{3}{2}g'_{zz}\beta B & \frac{\sqrt{3}}{2}(g'_{xz} - ig'_{yz})\beta B & \sqrt{3}E & 0 \\ \frac{\sqrt{3}}{2}(g'_{xz} + ig'_{yz})\beta B & -D + \frac{1}{2}g'_{zz}\beta B & (g'_{xz} - ig'_{yz})\beta B & \sqrt{3}E \\ \sqrt{3}E & (g'_{xz} + ig'_{yz})\beta B & -D - \frac{1}{2}g'_{zz}\beta B & \frac{\sqrt{3}}{2}(g'_{xz} - ig'_{yz})\beta B \\ 0 & \sqrt{3}E & \frac{\sqrt{3}}{2}(g'_{xz} + ig'_{yz})\beta B & D - \frac{3}{2}g'_{zz}\beta B \end{pmatrix}$$

Note that the symmetry of the conjugate spin eigenfunctions is broken because of the non-collinearity of the \mathbf{g} -tensor in contrast to the collinear case. Thus, the secular equation becomes quartic as given by

$$\begin{aligned} x^4 - \left[2D^2 + 6E^2 + \frac{5}{2}(g'_{zz}\beta B)^2 + \frac{5}{2}(g'_{xz}{}^2 + g'_{yz}{}^2)(\beta B)^2 \right] x^2 \\ - \left[4D(g'_{zz}\beta B)^2 - 2D(g'_{xz}{}^2 + g'_{yz}{}^2)(\beta B)^2 + 6E(g'_{xz}{}^2 + g'_{yz}{}^2)(\beta B)^2 \right] x + (D^2 + 3E^2)^2 \\ - \frac{5}{2}D^2(g'_{zz}\beta B)^2 + \frac{9}{2}E^2(g'_{zz}\beta B)^2 + \frac{1}{4}D^2(g'_{xz}{}^2 + g'_{yz}{}^2)(\beta B)^2 \\ + 6DE(g'_{xz}{}^2 + g'_{yz}{}^2)(\beta B)^2 - \frac{9}{2}E^2(g'_{xz}{}^2 + g'_{yz}{}^2)(\beta B)^2 + \frac{9}{8}(g'_{zz}\beta B)^4 \\ + \frac{9}{8}(g'_{zz}\beta B)^2(g'_{xz}{}^2 + g'_{yz}{}^2)(\beta B)^2 + \frac{9}{16}(g'_{xz}{}^2 + g'_{yz}{}^2)^4(\beta B)^4 = 0 \end{aligned}$$

where the relevant eigenenergies are real. The exact eigenenergies E can be analytically solved as follows:

$$\begin{aligned} E &= \frac{1}{2} \left[\pm_1 \sqrt{u_0} \pm_2 \sqrt{-2p - u_0 \mp_1 \frac{2q}{\sqrt{u_0}}} \right] \quad (S1) \\ u_0 &= 2a_0 \cos\left(\frac{1}{3} \arccos \frac{b_0}{2a_0}\right) - \frac{2p}{3} \\ a_0 &= \frac{1}{3} \sqrt{p^2 + 12r} \\ b_0 &= \frac{2p^3 - 27q^2 + 72pr}{3p^2 + 36r} \\ p &= -2D^2 - 6E^2 - \frac{5}{2}(g'_{zz}\beta B)^2 - \frac{5}{2}(g'_{xz}{}^2 + g'_{yz}{}^2)(\beta B)^2 \\ q &= -4D(g'_{zz}\beta B)^2 + 2D(g'_{xz}{}^2 + g'_{yz}{}^2)(\beta B)^2 - 6E(g'_{xz}{}^2 + g'_{yz}{}^2)(\beta B)^2 \\ r &= (D^2 + 3E^2)^2 - \frac{5}{2}D^2(g'_{zz}\beta B)^2 + \frac{9}{2}E^2(g'_{zz}\beta B)^2 + \frac{1}{4}D^2(g'_{xz}{}^2 + g'_{yz}{}^2)(\beta B)^2 \\ &\quad + 6DE(g'_{xz}{}^2 + g'_{yz}{}^2)(\beta B)^2 - \frac{9}{2}E^2(g'_{xz}{}^2 + g'_{yz}{}^2)(\beta B)^2 + \frac{9}{8}(g'_{zz}\beta B)^4 \\ &\quad + \frac{9}{16}(g'_{zz}\beta B)^2(g'_{xz}{}^2 + g'_{yz}{}^2)(\beta B)^2 + \frac{9}{16}(g'_{xz}{}^2 + g'_{yz}{}^2)^4(\beta B)^4 \end{aligned}$$

The corresponding eigenfunctions can also be derived analytically. Thus, the any transition probabilities can be obtained. The relationships between the $g^{\text{eff-}}$ - and g^{true} -values for the transition relevant to the $|M_S\rangle$ dominant Kramers doublets become complex as expected for the non-collinearity effect due to the contributions from the other principal g -values such as g_x and g_y . Thus, we solve the simultaneous equations associated with the relationships from the other principal orientations in order to get the expressions between the $\mathbf{g}^{\text{eff-}}$ - and \mathbf{g}^{true} -tensors. It should be noted that the genuine Zeeman perturbation formalism below can afford more facile generalization, as described in the previous paper, [1] and useful approach to gain physical insights into the effects caused by the non-collinearity and the symmetry reduction of the conjugate spinfunctions caused by the additional Zeeman interaction terms.

For the other principal axis orientations such as for $\mathbf{B} // x$, as well known, the cyclic permutation of the subscripts for the axes, $D_z \rightarrow D_x, D_x \rightarrow D_y, D_y \rightarrow D_z$, gives the eigenvalues and functions relevant to the ZFS \mathbf{D} -tensor; i.e., for the static magnetic field \mathbf{B} parallel to the principal x -axis, $\mathbf{B} // x$, the transformation of $D \rightarrow 1/2(3E - D)$ and $E \rightarrow -$

$1/2(E + D)$, and for $\mathbf{B} // y$, $D \rightarrow -1/2(3E + D)$ and $E \rightarrow 1/2(E - D)$ under the definition of the D - and E -values give the expressions associated with the ZFS tensor, respectively. The transformation associated with the \mathbf{D} -tensor described in terms of the principal axis coordinate system is straightforward because there is no off-diagonal element of the tensor.

For the case of the non-collinearity, the equations above include the off-diagonal elements of the \mathbf{g} -tensors, and the effects of any change in the principal axis coordinate system on the transformation between two tensors, \mathbf{T} and \mathbf{T}' should be mentioned. The effects are described in terms of the general properties of the transformation, in which the direction cosines (a_{ik} 's) defining the relative orientation between the axes of the two tensors. The transformation associated with the present cyclic permutation with respect to the three orthogonal coordinate axes involves only three non-vanishing a_{ik} 's ($= 1$) for one cyclic permutation, proving that all the diagonal and off-diagonal elements can be transformed into the elements governed by the transformation rule, $T_{ij}' = \sum a_{ik} a_{jl} T_{kl}$ ($k, l = 1, 2, 3$). Thus, for the other principal axis orientations the transformation relevant to the \mathbf{g} -tensor can be carried out by the cyclic permutation of the subscripts for the x , y and z axis, i.e., for $\mathbf{B} // x$ the facile transformation, $z \rightarrow x$, $x \rightarrow y$, $y \rightarrow z$ affords the corresponding eigen-values/-functions in a straightforward manner. The global invariance of the $g^{\text{eff}}/g^{\text{true}}$ relationships with respect to the axis transformations holds for the non-collinear case. This is also true for the formulas derived on the genuine Zeeman perturbation treatment for the non-collinearity, described below.

In the genuine Zeeman perturbation treatment for $\mathbf{B} // z$, the Zeeman interaction terms appear in both the diagonal and off-diagonal elements, as given below:

$$\begin{pmatrix} \frac{3}{2}g'_{zz}\beta B & \frac{\sqrt{3}}{2}(g'_{xz} - ig'_{yz})\beta B & 0 & 0 \\ \frac{\sqrt{3}}{2}(g'_{xz} + ig'_{yz})\beta B & \frac{1}{2}g'_{zz}\beta B & (g'_{xz} - ig'_{yz})\beta B & 0 \\ 0 & (g'_{xz} + ig'_{yz})\beta B & -\frac{1}{2}g'_{zz}\beta B & \frac{\sqrt{3}}{2}(g'_{xz} - ig'_{yz})\beta B \\ 0 & 0 & \frac{\sqrt{3}}{2}(g'_{xz} + ig'_{yz})\beta B & -\frac{3}{2}g'_{zz}\beta B \end{pmatrix}$$

The exact and analytical eigen-values/-functions for the ZFS Hamiltonian are derived in the previous paper [1], as the eigenfunctions are given as

$$\begin{aligned} \left| \varphi_{\pm \frac{3}{2}}^{(0)} \right\rangle &= \cos \delta \left| \pm \frac{3}{2} \right\rangle \pm \sin \delta \left| \mp \frac{1}{2} \right\rangle \\ \left| \varphi_{\pm \frac{1}{2}}^{(0)} \right\rangle &= \cos \delta \left| \pm \frac{1}{2} \right\rangle \mp \sin \delta \left| \mp \frac{3}{2} \right\rangle \end{aligned}$$

with $\tan 2\delta = \frac{\sqrt{3}E}{D}$. We describe the perturbing electronic Zeeman Hamiltonian in terms of the ZFS-based eigenfunctions, as follows:

$$\begin{pmatrix} G_{1z} & G_{3x} - iG_{3y} & -G_{3z} & G_{1x} - iG_{1y} \\ G_{3x} + iG_{3y} & G_{2z} & G_{2x} - iG_{2y} & G_{3z} \\ -G_{3z} & G_{2x} + iG_{2y} & -G_{2z} & G_{4x} - iG_{4y} \\ G_{1x} + iG_{1y} & G_{3z} & G_{4x} + iG_{4y} & -G_{1z} \end{pmatrix}$$

$$\begin{aligned} G_{1z} &= \frac{g'_{zz}\beta B}{2} (3 \cos^2 \delta - \sin^2 \delta) \\ G_{2z} &= \frac{g'_{zz}\beta B}{2} (\cos^2 \delta - 3 \sin^2 \delta) \\ G_{3z} &= g'_{zz}\beta B \sin 2\delta \\ G_{1x} &= \frac{g'_{xz}\beta B}{2} (\sqrt{3} \sin 2\delta - 2 \sin^2 \delta) \\ G_{1y} &= \frac{g'_{yz}\beta B}{2} (\sqrt{3} \sin 2\delta + 2 \sin^2 \delta) \end{aligned}$$

$$\begin{aligned}
G_{2x} &= \frac{g'_{xz}\beta B}{2} (2 \cos^2 \delta - \sqrt{3} \sin 2\delta) \\
G_{2y} &= \frac{g'_{yz}\beta B}{2} (2 \cos^2 \delta + \sqrt{3} \sin 2\delta) \\
G_{3x} &= \frac{g'_{xz}\beta B}{2} (\sqrt{3} \cos 2\delta + \sin 2\delta) \\
G_{3y} &= \frac{g'_{xz}\beta B}{2} (\sqrt{3} \cos 2\delta - \sin 2\delta) \\
G_{4x} &= \frac{g'_{xz}\beta B}{2} (\sqrt{3} \cos^2 \delta + 2 \sin 2\delta) \\
G_{4y} &= \frac{g'_{yz}\beta B}{2} (\sqrt{3} \cos^2 \delta - 2 \sin 2\delta)
\end{aligned}$$

Note that the spin states, $\left| \varphi_{\pm\frac{3}{2}}^{(0)} \right\rangle$ and $\left| \varphi_{\pm\frac{1}{2}}^{(0)} \right\rangle$ are degenerate, respectively. The relevant submatrices are

$$\begin{pmatrix} G_{1z} & G_{1x} - iG_{1y} \\ G_{1x} + iG_{1y} & -G_{1z} \end{pmatrix} \text{ for } \left| \varphi_{\pm\frac{3}{2}}^{(0)} \right\rangle$$

and

$$\begin{pmatrix} G_{2z} & G_{2x} - iG_{2y} \\ G_{2x} + iG_{2y} & -G_{2z} \end{pmatrix} \text{ for } \left| \varphi_{\pm\frac{1}{2}}^{(0)} \right\rangle.$$

The corresponding eigen-values/-functions are as follows:

$$\begin{aligned}
E_{1\pm} &= \pm \sqrt{G_{1x}^2 + G_{1y}^2 + G_{1z}^2} \\
\left| \varphi'_{+\frac{3}{2}} \right\rangle &= \cos \psi_1 \left| \varphi_{+\frac{3}{2}}^{(0)} \right\rangle + \sin \psi_1 e^{i\eta_1} \left| \varphi_{-\frac{3}{2}}^{(0)} \right\rangle \\
\left| \varphi'_{-\frac{3}{2}} \right\rangle &= \sin \psi_1 e^{-i\eta_1} \left| \varphi_{+\frac{3}{2}}^{(0)} \right\rangle - \cos \psi_1 \left| \varphi_{-\frac{3}{2}}^{(0)} \right\rangle
\end{aligned}$$

$$\begin{aligned}
E_{2\pm} &= \pm \sqrt{G_{2x}^2 + G_{2y}^2 + G_{2z}^2} \\
\left| \varphi'_{+\frac{1}{2}} \right\rangle &= \cos \psi_2 \left| \varphi_{+\frac{1}{2}}^{(0)} \right\rangle + \sin \psi_2 e^{i\eta_2} \left| \varphi_{-\frac{1}{2}}^{(0)} \right\rangle \\
\left| \varphi'_{-\frac{1}{2}} \right\rangle &= \sin \psi_2 e^{-i\eta_2} \left| \varphi_{+\frac{1}{2}}^{(0)} \right\rangle - \cos \psi_2 \left| \varphi_{-\frac{1}{2}}^{(0)} \right\rangle
\end{aligned}$$

with

$$\tan \psi_j = \frac{\sqrt{G_{jx}^2 + G_{jy}^2}}{G_{jz}}$$

and

$$\eta_j = \arg(G_{jx} + iG_{jy})$$

($j = 1, 2$). Then

$$\begin{pmatrix} \cos \psi_j & \sin \psi_j e^{-i\eta_j} \\ \sin \psi_j e^{i\eta_j} & -\cos \psi_j \end{pmatrix} \begin{pmatrix} G_{jz} & G_{jx} - iG_{jy} \\ G_{jx} + iG_{jy} & -G_{jz} \end{pmatrix} \begin{pmatrix} \cos \psi_j & \sin \psi_j e^{-i\eta_j} \\ \sin \psi_j e^{i\eta_j} & -\cos \psi_j \end{pmatrix}$$

$$= \begin{pmatrix} G_{jz} \cos 2\psi_j + (G_{jx} \cos \eta_j + G_{jy} \sin \eta_j) \sin 2\psi_j & G_{jz} \sin 2\psi_j e^{-i\eta_j} - (G_{jx} - iG_{jy}) \cos^2 \psi_j + (G_{jx} + iG_{jy}) \sin^2 \psi_j e^{-2i\eta_j} \\ G_{jz} \sin 2\psi_j e^{i\eta_j} - (G_{jx} + iG_{jy}) \cos^2 \psi_j + (G_{jx} - iG_{jy}) \sin^2 \psi_j e^{2i\eta_j} & -G_{jz} \cos 2\psi_j - (G_{jx} \cos \eta_j + G_{jy} \sin \eta_j) \sin 2\psi_j \end{pmatrix}$$

$$= \begin{pmatrix} \sqrt{G_{jx}^2 + G_{jy}^2 + G_{jz}^2} & 0 \\ 0 & -\sqrt{G_{jx}^2 + G_{jy}^2 + G_{jz}^2} \end{pmatrix}$$

The entire transformed Hamiltonian matrix for the electronic Zeeman is described as follows:

$$H' = \begin{pmatrix} H_{11} & H_{12} & H_{13} & 0 \\ H_{21} & H_{22} & 0 & H_{24} \\ H_{31} & 0 & H_{33} & H_{34} \\ 0 & H_{42} & H_{43} & H_{44} \end{pmatrix}$$

$$H_{11} = \sqrt{G_{1x}^2 + G_{1y}^2 + G_{1z}^2}$$

$$H_{22} = \sqrt{G_{2x}^2 + G_{2y}^2 + G_{2z}^2}$$

$$H_{33} = -\sqrt{G_{2x}^2 + G_{2y}^2 + G_{2z}^2}$$

$$H_{44} = -\sqrt{G_{1x}^2 + G_{1y}^2 + G_{1z}^2}$$

$$H_{12} = (G_{3x} - iG_{3y}) \cos \psi_1 \cos \psi_2 - G_{3z} \cos \psi_1 \sin \psi_2 e^{i\eta_2} + G_{3z} \cos \psi_2 \sin \psi_1 e^{-i\eta_1}$$

$$+ (G_{4x} + iG_{4y}) \sin \psi_1 \sin \psi_2 e^{-i(\eta_1 - \eta_2)}$$

$$H_{21} = H_{12}^*$$

$$H_{13} = G_{3z} \cos \psi_1 \cos \psi_2 + (G_{3x} - iG_{3y}) \cos \psi_1 \sin \psi_2 e^{-i\eta_2} - (G_{4x} + iG_{4y}) \cos \psi_2 \sin \psi_1 e^{-i\eta_1}$$

$$+ G_{3z} \sin \psi_1 \sin \psi_2 e^{-i(\eta_1 + \eta_2)}$$

$$H_{31} = H_{13}^*$$

$$H_{24} = -G_{3z} \cos \psi_1 \cos \psi_2 - (G_{4x} - iG_{4y}) \cos \psi_1 \sin \psi_2 e^{-i\eta_2} + (G_{3x} + iG_{3y}) \cos \psi_2 \sin \psi_1 e^{-i\eta_1}$$

$$- G_{3z} \sin \psi_1 \sin \psi_2 e^{-i(\eta_1 + \eta_2)}$$

$$H_{42} = H_{24}^*$$

$$H_{34} = (G_{4x} - iG_{4y}) \cos \psi_1 \cos \psi_2 - G_{3z} \cos \psi_1 \sin \psi_2 e^{i\eta_2} + G_{3z} \cos \psi_2 \sin \psi_1 e^{-i\eta_1}$$

$$+ (G_{3x} + iG_{3y}) \sin \psi_1 \sin \psi_2 e^{-i(\eta_1 - \eta_2)}$$

$$H_{43} = H_{34}^*$$

For $\mathbf{B} // z$, the eigenenergies to the third order in the genuine Zeeman perturbation treatment for the non-collinearity case are given as follows:

$$E_{+\frac{3}{2}} = D^* + \sqrt{G_{1x}^2 + G_{1y}^2 + G_{1z}^2} + \frac{|H_{12}|^2 + |H_{13}|^2}{2D^*} + \frac{|H_{12}|^2(H_{22} - H_{11}) + |H_{13}|^2(H_{33} - H_{11})}{4D^{*2}} \quad (\text{S2a})$$

$$E_{+\frac{1}{2}} = -D^* + \sqrt{G_{2x}^2 + G_{2y}^2 + G_{2z}^2} - \frac{|H_{21}|^2 + |H_{24}|^2}{2D^*} + \frac{|H_{21}|^2(H_{11} - H_{22}) + |H_{24}|^2(H_{44} - H_{22})}{4D^{*2}} \quad (\text{S2b})$$

$$E_{-\frac{1}{2}} = -D^* - \sqrt{G_{2x}^2 + G_{2y}^2 + G_{2z}^2} - \frac{|H_{31}|^2 + |H_{34}|^2}{2D^*} + \frac{|H_{31}|^2(H_{11} - H_{33}) + |H_{34}|^2(H_{44} - H_{33})}{4D^{*2}} \quad (\text{S2c})$$

$$E_{-\frac{3}{2}} = D^* - \sqrt{G_{1x}^2 + G_{1y}^2 + G_{1z}^2} + \frac{|H_{42}|^2 + |H_{43}|^2}{2D^*} + \frac{|H_{42}|^2(H_{22} - H_{44}) + |H_{43}|^2(H_{33} - H_{44})}{4D^{*2}} \quad (\text{S2d})$$

with $D^* = (D^2 + 3E^2)^{1/2}$. The eigenfunctions are obtained to the second order, which are not given here. Thus, the relationships within the Kramers doublets between the \mathbf{g}^{eff} - and \mathbf{g}^{true} -tensors for the non-collinearity for $\mathbf{B} // z$ are analytically derived, indicating that the symmetry reduction due to the non-collinearity requires solving the simultaneous higher-order algebraic equations for the relationships. The analytical expressions, as a function of E/D , for the relationships between the \mathbf{g}^{eff} - and \mathbf{g}^{true} -tensors in the case of the non-collinearity can be acquired by considering the

energies above at least to the second order under the assumption $|E_{+M_S} - E_{-M_S}| = g_z^{\text{eff}}\beta B$ for the Kramers doublets $|\pm M_S\rangle$.

For the other principal orientations, all the formulas of the corresponding eigen-energies/-functions can be derived by executing the cyclic permutations as described above.

1.2 Spin-sextet state ($S = 5/2$)

The matrix representation of the rank-2 ZFS tensor + electronic Zeeman interaction Hamiltonian for $S = 5/2$ is given for $B//z$ in the $|M_S\rangle$ basis set as

$$H_{\text{ZFS}+eZ} = \begin{pmatrix} \frac{10}{3}D + \frac{5}{2}g'_{zz}\beta B & \frac{\sqrt{5}}{2}(g'_{xz} - ig'_{yz})\beta B & \sqrt{10}E & 0 & 0 & 0 \\ \frac{\sqrt{5}}{2}(g'_{xz} + ig'_{yz})\beta B & -\frac{2}{3}D + \frac{3}{2}g'_{zz}\beta B & \sqrt{2}(g'_{xz} - ig'_{yz})\beta B & 3\sqrt{2}E & 0 & 0 \\ \sqrt{10}E & \sqrt{2}(g'_{xz} + ig'_{yz})\beta B & -\frac{8}{3}D + \frac{1}{2}g'_{zz}\beta B & \frac{3}{2}(g'_{xz} - ig'_{xy})\beta B & 3\sqrt{2}E & 0 \\ 0 & 3\sqrt{2}E & \frac{3}{2}(g'_{xz} + ig'_{yz})\beta B & -\frac{8}{3}D - \frac{1}{2}g'_{zz}\beta B & \sqrt{2}(g'_{xz} - ig'_{yz})\beta B & \sqrt{10}E \\ 0 & 0 & 3\sqrt{2}E & \sqrt{2}(g'_{xz} + ig'_{yz})\beta B & -\frac{2}{3}D - \frac{3}{2}g'_{zz}\beta B & \frac{\sqrt{5}}{2}(g'_{xz} - ig'_{yz})\beta B \\ 0 & 0 & 0 & \sqrt{10}E & \frac{\sqrt{5}}{2}(g'_{xz} + ig'_{yz})\beta B & \frac{10}{3}D - \frac{5}{2}g'_{zz}\beta B \end{pmatrix}$$

where the \mathbf{g} - and rank-2 ZFS tensors are assumed to be non-collinear, as the relative orientation between the two tensors defined in 1.1. The symmetry reduction due to the non-collinearity cannot provide us with analytical algebraic solutions of the eigen-value/-functions for the above Hamiltonian in contrast to the collinear case. The alternative approach based on the genuine Zeeman perturbation treatment affords extremely accurate solutions to the spin Hamiltonians composed of the rank-2 ZFS tensor + electronic Zeeman interaction terms, [1] and thus we invoke the genuine Zeeman perturbation approach to solve the eigen-values/-functions of the above Hamiltonian. The exact and analytical solutions for the eigen-values/-functions of the rank-2 ZFS Hamiltonian for $S = 5/2$ have already been derived, and the electronic Zeeman interaction Hamiltonian H_{eZ} in the $|M_S\rangle$ basis set is given as follows:

$$H_{eZ} = \begin{pmatrix} \frac{5}{2}g'_{zz}\beta B & \frac{\sqrt{5}}{2}(g'_{xz} - ig'_{yz})\beta B & 0 & 0 & 0 & 0 \\ \frac{\sqrt{5}}{2}(g'_{xz} + ig'_{yz})\beta B & \frac{3}{2}g'_{zz}\beta B & \sqrt{2}(g'_{xz} - ig'_{yz})\beta B & 0 & 0 & 0 \\ 0 & \sqrt{2}(g'_{xz} + ig'_{yz})\beta B & \frac{1}{2}g'_{zz}\beta B & \frac{3}{2}(g'_{xz} - ig'_{xy})\beta B & \sqrt{2}(g'_{xz} - ig'_{yz})\beta B & 0 \\ 0 & 0 & \frac{3}{2}(g'_{xz} + ig'_{yz})\beta B & -\frac{1}{2}g'_{zz}\beta B & -\frac{3}{2}g'_{zz}\beta B & \frac{\sqrt{5}}{2}(g'_{xz} - ig'_{yz})\beta B \\ 0 & 0 & 0 & \sqrt{2}(g'_{xz} + ig'_{yz})\beta B & \frac{\sqrt{5}}{2}(g'_{xz} + ig'_{yz})\beta B & -\frac{5}{2}g'_{zz}\beta B \\ 0 & 0 & 0 & 0 & \frac{\sqrt{5}}{2}(g'_{xz} + ig'_{yz})\beta B & -\frac{5}{2}g'_{zz}\beta B \end{pmatrix}$$

The exact spin eigenfunctions for the ZFS Hamiltonian, which are composed of the three pairs of the spin conjugate functions, are described as

$$\begin{aligned} |\varphi_{n+}^{(0)}\rangle &= \alpha_n \left| +\frac{5}{2} \right\rangle + \beta_n \left| -\frac{3}{2} \right\rangle + \gamma_n \left| +\frac{1}{2} \right\rangle \\ |\varphi_{n-}^{(0)}\rangle &= \alpha_n \left| -\frac{5}{2} \right\rangle + \beta_n \left| +\frac{3}{2} \right\rangle + \gamma_n \left| -\frac{1}{2} \right\rangle \end{aligned}$$

where $n = 0, 2$, and 1 denote the $|M_S = \pm 5/2\rangle$, $|\pm 3/2\rangle$ and $|\pm 1/2\rangle$ -dominant state, respectively, with the definitions of the coefficients given below. The corresponding exact eigenenergies $\varepsilon_n^{(0)}$ are given in the trigonometric functions.

$$\begin{aligned} \frac{\alpha_n}{\gamma_n} &= \frac{\sqrt{10}E}{\varepsilon_n^{(0)} - \frac{10}{3}D}, \quad \frac{\beta_n}{\gamma_n} = \frac{3\sqrt{2}E}{\varepsilon_n^{(0)} + \frac{2}{3}D}, \quad \gamma_n^2 = \left[\frac{10E^2}{(\varepsilon_n^{(0)} - \frac{10}{3}D)^2} + \frac{18E^2}{(\varepsilon_n^{(0)} + \frac{2}{3}D)^2} + 1 \right]^{-1} \\ \varepsilon_n^{(0)} &= 2a \cos\left(\frac{1}{3} \arccos \frac{b}{2a} + \frac{2n\pi}{3}\right) \quad (n = 0, 1, 2) \\ a &= \frac{2\sqrt{7}}{3} \sqrt{D^2 + 3E^2} \\ b &= \frac{40D(D^2 - 9E^2)}{21(D^2 + 3E^2)} \end{aligned}$$

The matrix elements of the new perturbing Hamiltonian matrix H_{pert} described in the $|\varphi_{n+}^{(0)}\rangle$ and $|\varphi_{n-}^{(0)}\rangle$ basis set are given as follows. Within $\{+5/2, -3/2, +1/2\}$, the matrix elements are given as

$$\langle \varphi_{m+}^{(0)} | H_{\text{pert}} | \varphi_{n+}^{(0)} \rangle = G_{zz,mn}$$

and within $\{-5/2, +3/2, -1/2\}$, they are as follows:

$$\langle \varphi_{m-}^{(0)} | H_{\text{pert}} | \varphi_{n-}^{(0)} \rangle = -G_{zz,mn}$$

The matrix elements between the spin conjugate states are given as

$$\begin{aligned} \langle \varphi_{m+}^{(0)} | H_{\text{pert}} | \varphi_{n-}^{(0)} \rangle &= G_{xz,mn} - iG_{yz,mn} \\ \langle \varphi_{m-}^{(0)} | H_{\text{pert}} | \varphi_{n+}^{(0)} \rangle &= G_{xz,mn} + iG_{yz,mn} \end{aligned}$$

with the following definitions:

$$\begin{aligned} G_{zz,mn} &= \frac{g'_{zz}\beta B}{2} (5\alpha_m\alpha_n - 3\beta_m\beta_n + \gamma_m\gamma_n) \\ G_{xz,mn} &= \frac{g'_{xz}\beta B}{2} (\sqrt{5}\alpha_m\beta_n + \sqrt{5}\beta_m\alpha_n + 2\sqrt{2}\beta_m\gamma_n + 2\sqrt{2}\gamma_m\beta_n + 3\gamma_m\gamma_n) \\ G_{yz,mn} &= \frac{g'_{yz}\beta B}{2} (\sqrt{5}\alpha_m\beta_n + \sqrt{5}\beta_m\alpha_n - 2\sqrt{2}\beta_m\gamma_n - 2\sqrt{2}\gamma_m\beta_n + 3\gamma_m\gamma_n) \end{aligned}$$

Noting that the Kramers doublet states, i.e., the $|\varphi_{\pm\frac{5}{2}}^{(0)}\rangle$, $|\varphi_{\pm\frac{3}{2}}^{(0)}\rangle$ and $|\varphi_{\pm\frac{1}{2}}^{(0)}\rangle$ dominant states are degenerate, respectively, we diagonalize the following two by two matrix and lift the degeneracy,

$$\begin{pmatrix} G_{zz,nn} & G_{xz,nn} - iG_{yz,nn} \\ G_{xz,nn} + iG_{yz,nn} & -G_{zz,nn} \end{pmatrix}$$

where nm is replaced with n for simplicity and $n = 0, 2$ and 1 stand for the $|\varphi_{\pm\frac{5}{2}}^{(0)}\rangle$, $|\varphi_{\pm\frac{3}{2}}^{(0)}\rangle$ and $|\varphi_{\pm\frac{1}{2}}^{(0)}\rangle$ dominant spin state. Similar to the case of $S = 3/2$, the eigen-energies and -functions are given as

$$\begin{aligned} E_{n\pm} &= \pm \sqrt{G_{xz,n}^2 + G_{yz,n}^2 + G_{zz,n}^2} \\ |\varphi'_{+M_S}\rangle &= \cos \psi_n |\varphi_{+M_S}^{(0)}\rangle + \sin \psi_n e^{i\eta_n} |\varphi_{-M_S}^{(0)}\rangle \\ |\varphi'_{-M_S}\rangle &= \sin \psi_n e^{-i\eta_n} |\varphi_{+M_S}^{(0)}\rangle - \cos \psi_n |\varphi_{-M_S}^{(0)}\rangle \end{aligned}$$

with

$$\begin{aligned} \tan \psi_n &= \frac{\sqrt{G_{xz,n}^2 + G_{yz,n}^2}}{G_{zz,n}} \\ \eta_n &= \arg(G_{xz,n} + iG_{yz,n}) \end{aligned}$$

and $n = 0, 2, 1$. The transformed electronic Zeeman interaction Hamiltonian H' for Rayleigh-Schrödinger perturbation treatment is given as

$$H' = \begin{pmatrix} H'_{11} & H'_{12} & H'_{13} & H'_{14} & H'_{15} & 0 \\ H'_{21} & H'_{22} & H'_{23} & H'_{24} & 0 & H'_{26} \\ H'_{31} & H'_{32} & H'_{33} & 0 & H'_{35} & H'_{36} \\ H'_{41} & H'_{42} & 0 & H'_{44} & H'_{45} & H'_{46} \\ H'_{51} & 0 & H'_{53} & H'_{54} & H'_{55} & H'_{56} \\ 0 & H'_{62} & H'_{63} & H'_{64} & H'_{65} & H'_{66} \end{pmatrix}$$

$$H'_{11} = \sqrt{G_{xz,0}^2 + G_{yz,0}^2 + G_{zz,0}^2}$$

$$H'_{22} = \sqrt{G_{xz,2}^2 + G_{yz,2}^2 + G_{zz,2}^2}$$

$$H'_{33} = \sqrt{G_{xz,1}^2 + G_{yz,1}^2 + G_{zz,1}^2}$$

$$H'_{44} = -\sqrt{G_{xz,1}^2 + G_{yz,1}^2 + G_{zz,1}^2}$$

$$H'_{55} = -\sqrt{G_{xz,2}^2 + G_{yz,2}^2 + G_{zz,2}^2}$$

$$H'_{66} = -\sqrt{G_{xz,0}^2 + G_{yz,0}^2 + G_{zz,0}^2}$$

$$H'_{12} = G_{zz,02}(\cos \psi_0 \sin \psi_2 e^{i\eta_2} - \sin \psi_0 e^{i\eta_0} \cos \psi_2) + G_{xz,02}(\cos \psi_0 \cos \psi_2 + \sin \psi_0 \sin \psi_2 e^{i(\eta_0+\eta_2)}) - iG_{yz,02}(\cos \psi_0 \cos \psi_2 - \sin \psi_0 \sin \psi_2 e^{i(\eta_0+\eta_2)})$$

$$H'_{21} = H'_{12}^*$$

$$H'_{13} = G_{zz,01}(\cos \psi_0 \cos \psi_1 + \sin \psi_0 \sin \psi_1 e^{i(\eta_0+\eta_1)}) + G_{xz,01}(\cos \psi_0 \sin \psi_1 e^{i\eta_1} + \sin \psi_0 e^{i\eta_0} \cos \psi_1) - iG_{yz,01}(\cos \psi_0 \sin \psi_1 e^{i\eta_1} - \sin \psi_0 e^{i\eta_0} \cos \psi_1)$$

$$H'_{31} = H'_{13}^*$$

$$H'_{14} = G_{zz,01}(\cos \psi_0 \sin \psi_1 e^{i\eta_1} + \sin \psi_0 e^{i\eta_0} \cos \psi_1) - G_{xz,01}(\cos \psi_0 \cos \psi_1 - \sin \psi_0 \sin \psi_1 e^{i(\eta_0-\eta_1)}) + iG_{yz,01}(\cos \psi_0 \cos \psi_1 + \sin \psi_0 \sin \psi_1 e^{i(\eta_0-\eta_1)})$$

$$H'_{41} = H'_{14}^*$$

$$H'_{15} = G_{zz,02}(\cos \psi_0 \cos \psi_2 - \sin \psi_0 \sin \psi_2 e^{i(\eta_0-\eta_2)}) + G_{xz,02}(\cos \psi_0 \sin \psi_2 e^{-i\eta_2} - \sin \psi_0 e^{i\eta_0} \cos \psi_2) - iG_{yz,02}(\cos \psi_0 \sin \psi_2 e^{-i\eta_2} + \sin \psi_0 e^{i\eta_0} \cos \psi_2)$$

$$H'_{51} = H'_{15}^*$$

$$H'_{23} = -G_{zz,21}(\cos \psi_2 \sin \psi_1 e^{i\eta_1} - \sin \psi_2 e^{i\eta_2} \cos \psi_1) + G_{xz,21}(\cos \psi_2 \cos \psi_1 + \sin \psi_2 \sin \psi_1 e^{i(\eta_2+\eta_1)}) + iG_{yz,21}(\cos \psi_2 \cos \psi_1 - \sin \psi_2 \sin \psi_1 e^{i(\eta_2+\eta_1)})$$

$$H'_{32} = H'_{23}^*$$

$$H'_{24} = G_{zz,21}(\cos \psi_2 \cos \psi_1 + \sin \psi_2 \sin \psi_1 e^{-i(\eta_1-\eta_2)}) + G_{xz,21}(\cos \psi_2 \sin \psi_1 e^{-i\eta_1} - \sin \psi_2 e^{i\eta_2} \cos \psi_1) + iG_{yz,21}(\cos \psi_2 \sin \psi_1 e^{-i\eta_1} + \sin \psi_2 e^{i\eta_2} \cos \psi_1)$$

$$H'_{42} = H'_{24}^*$$

$$H'_{26} = G_{zz,20}(\cos \psi_2 \cos \psi_0 + \sin \psi_2 \sin \psi_0 e^{i(\eta_2-\eta_0)}) + G_{xz,20}(\cos \psi_2 \sin \psi_0 e^{-i\eta_0} - \sin \psi_2 e^{i\eta_2} \cos \psi_0) + iG_{yz,20}(\cos \psi_2 \sin \psi_0 e^{-i\eta_0} + \sin \psi_2 e^{i\eta_2} \cos \psi_0)$$

$$H'_{62} = H'_{26}^*$$

$$H'_{35} = -G_{zz,12}(\cos \psi_1 \cos \psi_2 + \sin \psi_1 \sin \psi_2 e^{i(\eta_1-\eta_2)}) + G_{xz,12}(\cos \psi_1 \sin \psi_2 e^{-i\eta_2} - \sin \psi_1 e^{i\eta_1} \cos \psi_2) + iG_{yz,12}(\cos \psi_1 \sin \psi_2 e^{-i\eta_2} + \sin \psi_1 e^{i\eta_1} \cos \psi_2)$$

$$H'_{53} = H'_{35}^*$$

$$H'_{36} = G_{zz,10}(\cos \psi_1 \sin \psi_0 e^{-i\eta_0} + \sin \psi_1 e^{i\eta_1} \cos \psi_0) - G_{xz,10}(\cos \psi_1 \cos \psi_0 - \sin \psi_1 \sin \psi_0 e^{i(\eta_1 - \eta_0)}) \\ + iG_{yz,10}(\cos \psi_1 \cos \psi_0 + \sin \psi_1 \sin \psi_0 e^{i(\eta_1 - \eta_0)}) \\ H'_{63} = H'_{36}^*$$

$$H'_{45} = G_{zz,12}(\cos \psi_1 \sin \psi_2 e^{-i\eta_2} - \sin \psi_1 e^{i\eta_1} \cos \psi_2) + G_{xz,12}(\cos \psi_1 \cos \psi_2 - \sin \psi_1 \sin \psi_2 e^{i(\eta_1 - \eta_2)}) \\ + iG_{yz,12}(\cos \psi_1 \cos \psi_2 + \sin \psi_1 \sin \psi_2 e^{i(\eta_1 - \eta_2)}) \\ H'_{54} = H'_{45}^*$$

$$H'_{46} = -G_{zz,10}(\cos \psi_1 \cos \psi_0 - \sin \psi_1 \sin \psi_0 e^{-i(\eta_1 + \eta_2)}) - G_{xz,10}(\cos \psi_1 \sin \psi_0 e^{-i\eta_0} - \cos \psi_0 \sin \psi_1 e^{-i\eta_1}) \\ - iG_{yz,10}(\cos \psi_1 \sin \psi_0 e^{-i\eta_0} + \cos \psi_0 \sin \psi_1 e^{-i\eta_1}) \\ H'_{64} = H'_{46}^*$$

$$H'_{56} = -G_{zz,20}(\cos \psi_2 \sin \psi_0 e^{-i\eta_0} - \sin \psi_2 e^{-i\eta_2} \cos \psi_0) + G_{xz,20}(\cos \psi_2 \cos \psi_0 + \sin \psi_2 \sin \psi_0 e^{-i(\eta_2 + \eta_0)}) \\ - iG_{yz,20}(\cos \psi_2 \cos \psi_0 - \sin \psi_2 \sin \psi_0 e^{-i(\eta_2 + \eta_0)}) \\ H'_{65} = H'_{56}^*$$

The eigenenergies of the $|M_S\rangle$ dominant states to the third order are derived as follows, where only the energies are explicitly described below and the eigenfunctions given to the second order:

$$E_{+\frac{5}{2}} \\ = \varepsilon_0^{(0)} + \sqrt{G_{xz,0}^2 + G_{yz,0}^2 + G_{zz,0}^2} + \frac{|H'_{12}|^2 + |H'_{15}|^2}{\varepsilon_0^{(0)} - \varepsilon_2^{(0)}} + \frac{|H'_{13}|^2 + |H'_{14}|^2}{\varepsilon_0^{(0)} - \varepsilon_1^{(0)}} + \frac{|H'_{12}|^2(H'_{22} - H'_{11}) + |H'_{15}|^2(H'_{55} - H'_{11})}{(\varepsilon_0^{(0)} - \varepsilon_2^{(0)})^2} \\ + \frac{H'_{12}H'_{23}H'_{31} + H'_{12}H'_{24}H'_{41} + H'_{13}H'_{32}H'_{21} + H'_{13}H'_{35}H'_{51} + H'_{14}H'_{42}H'_{21} + H'_{14}H'_{45}H'_{51} + H'_{15}H'_{53}H'_{31} + H'_{15}H'_{54}H'_{41}}{(\varepsilon_0^{(0)} - \varepsilon_2^{(0)})(\varepsilon_0^{(0)} - \varepsilon_1^{(0)})} \\ + \frac{|H'_{13}|^2(H'_{33} - H'_{11}) + |H'_{14}|^2(H'_{44} - H'_{11})}{(\varepsilon_0^{(0)} - \varepsilon_1^{(0)})^2}$$

$$E_{+\frac{3}{2}} \\ = \varepsilon_2^{(0)} + \sqrt{G_{xz,2}^2 + G_{yz,2}^2 + G_{zz,2}^2} + \frac{|H'_{21}|^2 + |H'_{26}|^2}{\varepsilon_2^{(0)} - \varepsilon_0^{(0)}} + \frac{|H'_{23}|^2 + |H'_{24}|^2}{\varepsilon_2^{(0)} - \varepsilon_1^{(0)}} + \frac{|H'_{21}|^2(H'_{11} - H'_{22}) + |H'_{26}|^2(H'_{66} - H'_{22})}{(\varepsilon_2^{(0)} - \varepsilon_0^{(0)})^2} \\ + \frac{H'_{21}H'_{13}H'_{32} + H'_{21}H'_{14}H'_{42} + H'_{23}H'_{31}H'_{12} + H'_{23}H'_{36}H'_{62} + H'_{24}H'_{41}H'_{12} + H'_{24}H'_{46}H'_{62} + H'_{26}H'_{63}H'_{32} + H'_{26}H'_{64}H'_{42}}{(\varepsilon_2^{(0)} - \varepsilon_0^{(0)})(\varepsilon_2^{(0)} - \varepsilon_1^{(0)})} \\ + \frac{|H'_{23}|^2(H'_{33} - H'_{22}) + |H'_{24}|^2(H'_{44} - H'_{22})}{(\varepsilon_2^{(0)} - \varepsilon_1^{(0)})^2}$$

$$E_{+\frac{1}{2}} \\ = \varepsilon_1^{(0)} + \sqrt{G_{xz,1}^2 + G_{yz,1}^2 + G_{zz,1}^2} + \frac{|H'_{31}|^2 + |H'_{36}|^2}{\varepsilon_1^{(0)} - \varepsilon_0^{(0)}} + \frac{|H'_{32}|^2 + |H'_{35}|^2}{\varepsilon_1^{(0)} - \varepsilon_2^{(0)}} + \frac{|H'_{31}|^2(H'_{11} - H'_{33}) + |H'_{36}|^2(H'_{66} - H'_{33})}{(\varepsilon_1^{(0)} - \varepsilon_0^{(0)})^2} \\ + \frac{H'_{31}H'_{12}H'_{23} + H'_{31}H'_{15}H'_{53} + H'_{32}H'_{21}H'_{13} + H'_{32}H'_{26}H'_{63} + H'_{35}H'_{51}H'_{13} + H'_{35}H'_{56}H'_{63} + H'_{36}H'_{62}H'_{23} + H'_{36}H'_{65}H'_{53}}{(\varepsilon_1^{(0)} - \varepsilon_0^{(0)})(\varepsilon_1^{(0)} - \varepsilon_2^{(0)})} \\ + \frac{|H'_{32}|^2(H'_{22} - H'_{33}) + |H'_{35}|^2(H'_{55} - H'_{33})}{(\varepsilon_1^{(0)} - \varepsilon_2^{(0)})^2}$$

$$E_{-\frac{1}{2}} \\ = \varepsilon_1^{(0)} - \sqrt{G_{xz,1}^2 + G_{yz,1}^2 + G_{zz,1}^2} + \frac{|H'_{41}|^2 + |H'_{46}|^2}{\varepsilon_1^{(0)} - \varepsilon_0^{(0)}} + \frac{|H'_{42}|^2 + |H'_{45}|^2}{\varepsilon_1^{(0)} - \varepsilon_2^{(0)}} + \frac{|H'_{41}|^2(H'_{11} - H'_{44}) + |H'_{46}|^2(H'_{66} - H'_{44})}{(\varepsilon_1^{(0)} - \varepsilon_0^{(0)})^2} \\ + \frac{H'_{41}H'_{12}H'_{24} + H'_{41}H'_{15}H'_{54} + H'_{42}H'_{21}H'_{14} + H'_{42}H'_{26}H'_{63} + H'_{45}H'_{51}H'_{14} + H'_{45}H'_{56}H'_{64} + H'_{46}H'_{62}H'_{24} + H'_{46}H'_{65}H'_{54}}{(\varepsilon_1^{(0)} - \varepsilon_0^{(0)})(\varepsilon_1^{(0)} - \varepsilon_2^{(0)})} \\ + \frac{|H'_{42}|^2(H'_{22} - H'_{44}) + |H'_{45}|^2(H'_{55} - H'_{44})}{(\varepsilon_1^{(0)} - \varepsilon_0^{(0)})^2}$$

$$E_{-\frac{3}{2}} \\ = \varepsilon_2^{(0)} - \sqrt{G_{xz,2}^2 + G_{yz,2}^2 + G_{zz,2}^2} + \frac{|H'_{51}|^2 + |H'_{56}|^2}{\varepsilon_2^{(0)} - \varepsilon_0^{(0)}} + \frac{|H'_{53}|^2 + |H'_{54}|^2}{\varepsilon_2^{(0)} - \varepsilon_1^{(0)}} + \frac{|H'_{51}|^2(H'_{11} - H'_{55}) + |H'_{56}|^2(H'_{66} - H'_{55})}{(\varepsilon_2^{(0)} - \varepsilon_0^{(0)})^2} \\ + \frac{H'_{51}H'_{13}H'_{35} + H'_{51}H'_{14}H'_{45} + H'_{53}H'_{31}H'_{15} + H'_{53}H'_{36}H'_{65} + H'_{54}H'_{41}H'_{15} + H'_{54}H'_{46}H'_{65} + H'_{56}H'_{63}H'_{35} + H'_{56}H'_{64}H'_{45}}{(\varepsilon_2^{(0)} - \varepsilon_0^{(0)})(\varepsilon_2^{(0)} - \varepsilon_1^{(0)})} \\ + \frac{|H'_{53}|^2(H'_{33} - H'_{55}) + |H'_{54}|^2(H'_{44} - H'_{55})}{(\varepsilon_2^{(0)} - \varepsilon_0^{(0)})^2}$$

$$\begin{aligned}
& E_{-\frac{5}{2}} \\
&= \varepsilon_0^{(0)} - \sqrt{G_{xz,0}^2 + G_{yz,0}^2 + G_{zz,0}^2} + \frac{|H'_{62}|^2 + |H'_{65}|^2}{\varepsilon_0^{(0)} - \varepsilon_2^{(0)}} + \frac{|H'_{63}|^2 + |H'_{64}|^2}{\varepsilon_0^{(0)} - \varepsilon_1^{(0)}} + \frac{|H'_{62}|^2(H'_{22} - H'_{66}) + |H'_{65}|^2(H'_{55} - H'_{66})}{(\varepsilon_0^{(0)} - \varepsilon_2^{(0)})^2} \\
&+ \frac{H'_{62}H'_{23}H'_{36} + H'_{62}H'_{24}H'_{46} + H'_{63}H'_{32}H'_{26} + H'_{63}H'_{35}H'_{56} + H'_{64}H'_{42}H'_{26} + H'_{64}H'_{45}H'_{56} + H'_{65}H'_{53}H'_{36} + H'_{65}H'_{54}H'_{46}}{(\varepsilon_0^{(0)} - \varepsilon_2^{(0)})(\varepsilon_0^{(0)} - \varepsilon_1^{(0)})} \\
&+ \frac{|H'_{63}|^2(H'_{33} - H'_{66}) + |H'_{64}|^2(H'_{44} - H'_{66})}{(\varepsilon_0^{(0)} - \varepsilon_1^{(0)})^2}
\end{aligned}$$

The analytical expressions, as a function of E/D , for the relationships between the \mathbf{g}^{eff} - and \mathbf{g}^{true} -tensors in the case of the non-collinearity can be acquired by considering the energies above at least to the second order. The procedure to derive the relationships is the same as described for $S = 3/2$.

For the other principal orientations, all the formulas of the corresponding eigen-energies/-functions can be derived by executing the cyclic permutations as described for the case of $S = 3/2$.

Model calculation for $S = 3/2$

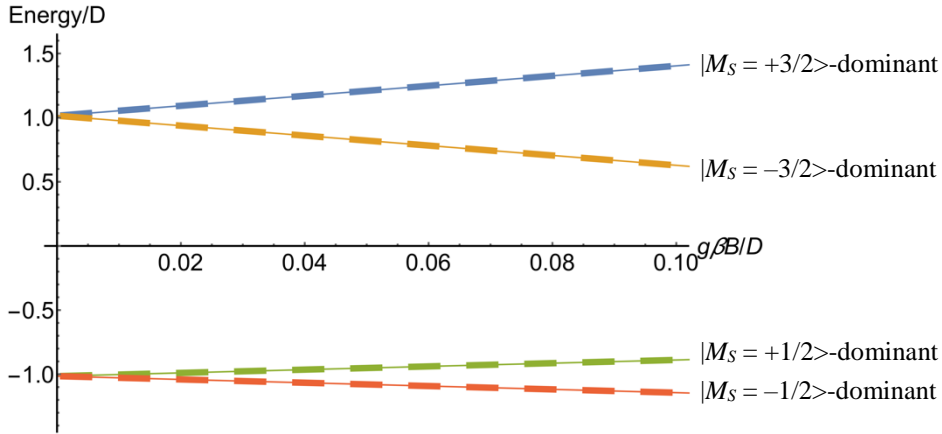


Fig. S1. Energy diagram of the spin states, denoted by M_S , based on both the exact solution (Eq. (S1), solid lines) and the genuine Zeeman perturbation approaches (up to the second-order terms in Eqs. (S2a)–(S2d), broken lines) for the non-collinear case with the static magnetic field \mathbf{B} parallel to the principal z -axis of the ZFS tensor. The set of Euler angles of the \mathbf{g} -tensor with respect to the ZFS tensor were $\alpha = 0^\circ$, $\beta = 90^\circ$ and $\gamma = 138^\circ$. The diagonal elements of the original principal coordinate \mathbf{g}' -tensor were $g_{x'} = 2.8$, $g_{y'} = 2.46$ and $g_{z'} = 2.8$. The ZFS parameter D was set to positive and $E/D = 0.1$.

2. Analyses of X-band fine-structure/hyperfine structure ESR spectra of complexes 1–3 revisited

(a) $[\text{Mn}^{\text{II}}(\text{TpivPP})\text{X}]$ (complex 1, X = 1-MeIm; complex 2, X = 2-MeHIm)

Table S1. The experimental g -values of complexes 1 and 2, as revisited and reanalyzed in this work in terms of the fictitious spin-1/2 and full spin Hamiltonian approaches for their X-band ESR spectra: The microwave frequency of 9.45 GHz was taken from the reported paper.

Sample	g^{eff} -values						g^{true} -values		
1, powder	5.9 ± 0.1	5.9 ± 0.1	1.93	1.24	0.774	0.543	2.18	2.14	1.93
2, powder	5.8 ± 0.1	5.8 ± 0.1	2.0	1.22	0.765	0.530	2.15	2.17	2.0
2, solution	5.9 ± 0.1	5.9 ± 0.1	1.96	1.23	0.770	0.540	2.19	2.12	1.96
	Principal x-canonical peak	Principal y-canonical peak	Principal z-canonical peak	Principal x- and y-canonical and off-axis extra peak	Off-axis extra peak	Off-axis extra peak	Principal x-canonical peak	Principal y-canonical peak	Principal z-canonical peak

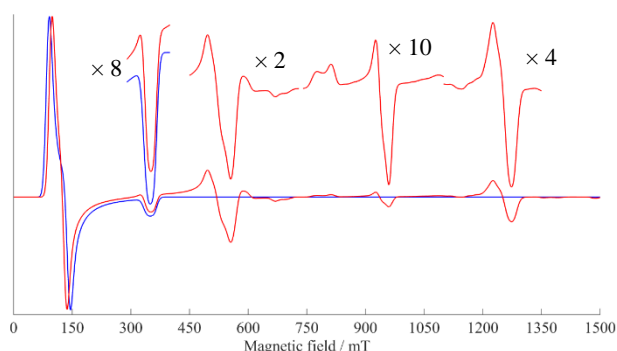


Fig. S2. The simulated X-band (9.45 GHz) ESR spectra of $[\text{Mn}^{\text{II}}(\text{TpivPP})(1\text{-MeIm})]$ (complex 1) in powder at 90 K based on both the fictitious spin-1/2 Hamiltonian and the full spin Hamiltonian which includes the rank-2 ZFS tensor. The microwave frequency of 9.45 GHz and temperature of 90 K were taken from the reported paper. [2] The fictitious spin-1/2 Hamiltonian parameters: The spectrum in blue; $S^{\text{eff}} = 1/2$, $g_{1,x}^{\text{eff}} = 5.9$, $g_{1,y}^{\text{eff}} = 5.9$, $g_{1,z}^{\text{eff}} = 1.93$, $A_{1,x}^{\text{eff}}(^{55}\text{Mn}) = 810$ MHz, $A_{1,y}^{\text{eff}}(^{55}\text{Mn}) = 660$ MHz and $A_{1,z}^{\text{eff}}(^{55}\text{Mn}) = 150$ MHz. The full spin Hamiltonian parameters: The spectrum in red; $S = 5/2$, $g_x = 2.18$, $g_y = 2.14$, $g_z = 1.93$, $A_x(^{55}\text{Mn}) = 300$ MHz, $A_y(^{55}\text{Mn}) = 295$ MHz, $A_z(^{55}\text{Mn}) = 150$ MHz, $D = 20.6$ GHz and $E/D = 0.002$ with the peak-to-peak linewidth of the single transition = 14 mT. No strain effect on the linewidth was included. All the magnetic tensors were assumed to be collinear. The spectral simulations were obtained by using EasySpin (ver. 5.1.12). [3]

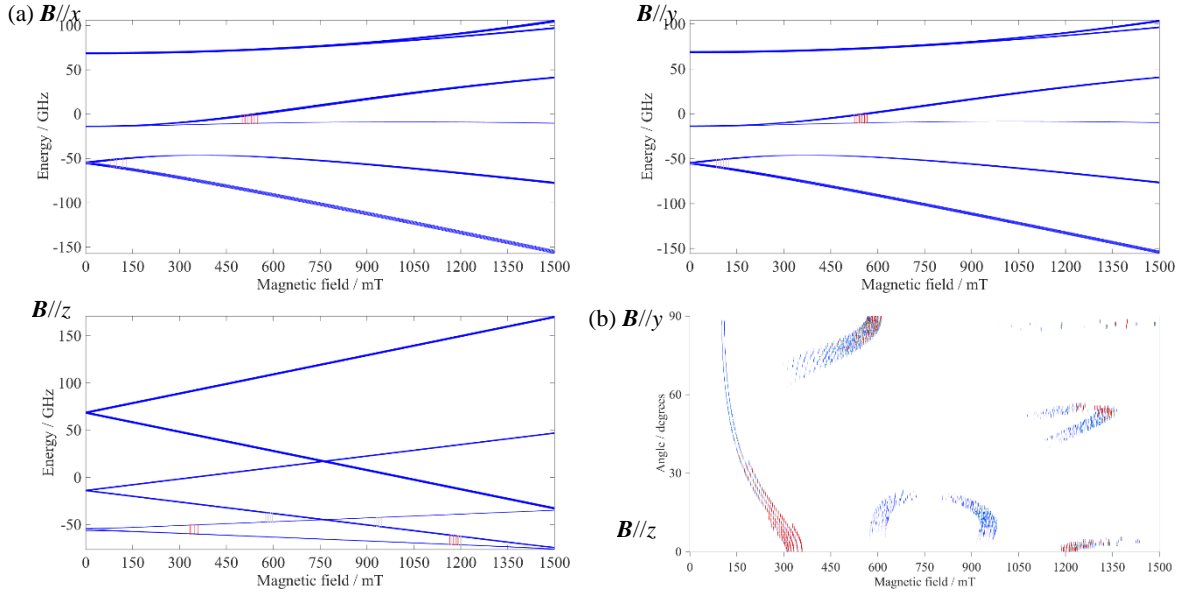


Fig. S3. (a) The energy diagrams of complex **1** for the principal axis orientations as a function of the magnitude of the static magnetic field and (b) the angular dependence of the resonance fields for complex **1** from the principal z -to- y -axis, based on the full spin Hamiltonian approach. The spin Hamiltonian parameters used for the simulations: $S = 5/2$, $g_x = 2.18$, $g_y = 2.14$, $g_z = 1.93$, $A_x(^{55}\text{Mn}) = 300$ MHz, $A_y(^{55}\text{Mn}) = 295$ MHz, $A_z(^{55}\text{Mn}) = 150$ MHz, $D = 20.6$ GHz and $E/D = 0.002$. The simulations were obtained by using EasySpin (ver. 5.1.12) [3] with varying the angle of the magnetic field one-degree stepwise. Note that the yz -plane angular dependence is chosen only for clarity, which reveals the clear appearance of the off-principal axis extra peaks. For the complete spectral simulation, all the orientations of the static magnetic field were considered to assign the peaks in the powder-pattern ESR spectra. (b) Colors denote the transition intensities.

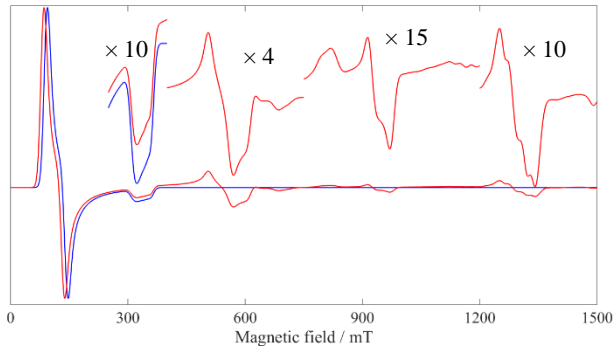


Fig. S4. The simulated X-band (9.45 GHz) ESR spectra of $[\text{Mn}^{\text{II}}(\text{TpivPP})(2\text{-MeHIm})]$ (complex **2**) in powder at 90 K based on both the fictitious spin-1/2 Hamiltonian and full spin Hamiltonian including the rank-2 ZFS tensor. The microwave frequency of 9.45 GHz and temperature of 90 K were taken from the reported paper. [2] The fictitious spin-1/2 Hamiltonian parameters: The spectrum in blue; $S^{\text{eff}} = 1/2$, $g_{1,x}^{\text{eff}} = 5.8$, $g_{1,y}^{\text{eff}} = 5.8$, $g_{1,z}^{\text{eff}} = 2.0$, $A_{1,x}^{\text{eff}}(^{55}\text{Mn}) = 750$ MHz, $A_{1,y}^{\text{eff}}(^{55}\text{Mn}) = 660$ MHz and $A_{1,z}^{\text{eff}}(^{55}\text{Mn}) = 270$ MHz. The full spin Hamiltonian parameters: The spectrum in red; $S = 5/2$, $g_x = 2.15$, $g_y = 2.07$, $g_z = 2.00$, $A_x(^{55}\text{Mn}) = 280$ MHz, $A_y(^{55}\text{Mn}) = 235$ MHz cm^{-1} , $A_z(^{55}\text{Mn}) = 270$ MHz, $D = 21.5$ GHz and $E/D = 0.005$ with the peak-to-peak linewidth for the single transition = 15 mT. No strain effect on the linewidth was included. All the magnetic tensors were assumed to be collinear. The simulated spectra were obtained using EasySpin (ver. 5.1.12). [3]

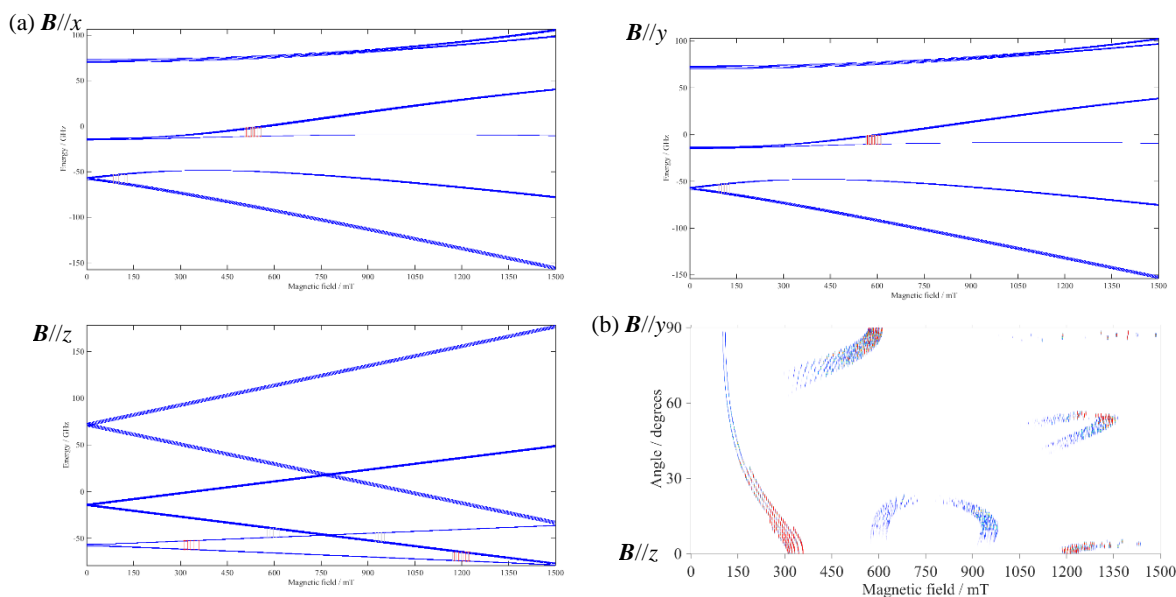


Fig. S5 (a) The energy diagrams of complex **2** for the principal axis orientations as a function of the magnitude of the static magnetic field and (b) the angular dependence of the resonance fields for complex **2** from the principal z -to- y -axis, based on the full spin Hamiltonian approach. The spin Hamiltonian parameters used for the simulations. $S = 5/2$, $g_x = 2.15$, $g_y = 2.07$, $g_z = 2.00$, $A_x(^{55}\text{Mn}) = 280$ MHz, $A_y(^{55}\text{Mn}) = 235$ MHz cm^{-1} , $A_z(^{55}\text{Mn}) = 270$ MHz, $D = 21.5$ GHz, $E/D = 0.005$. The simulations were obtained by using EasySpin (ver. 5.1.12) [3] with varying the angle of the magnetic field one-degree stepwise. Note that the yz -plane angular dependence is chosen only for clarity, which reveals the clear appearance of the off-principal axis extra peaks. For the complete spectral simulation, all the orientations of the static magnetic field were considered to assign the peaks in the powder-pattern ESR spectra.

Table S2. The experimental principal values and E/D of the experimental magnetic tensors of manganese complexes **1** and **2**, as determined in terms of the full spin Hamiltonian approach. The values are to be compared with the theoretical ones based on quantum chemical calculations.

	1 , powder	2 , powder	2 , glass solution
g_x	2.18	2.15	2.19
g_y	2.14	2.07	2.12
g_z	1.93	2.00	1.96
$A_x(^{55}\text{Mn})/\text{MHz}$	300	280	280
$A_y(^{55}\text{Mn})/\text{MHz}$	295	235	270
$A_z(^{55}\text{Mn})/\text{MHz}$	150	270	240
D/cm^{-1}	+0.69	+0.72	+0.70
$ E/D $	0.002	0.005	0.004

Table S3. The theoretical principal values and E/D of the magnetic tensors of manganese complexes **1** and **2**, as obtained by the quantum chemical calculations on the basis of the NOB-PK method at the UBP86/Sapporo-DZP, 3-21g level. The definitions of the principal axes are given in the text. Importantly, the theoretical D -values are predicted to be positive. The theoretical hyperfine principal values of $^{55}\text{Mn}(\text{II})$ are underestimated, and the ratios of the theoretical E/D values are overestimated, indicating that more rectified theoretical treatments of the magnetic tensors are required.

	1	2
g_{xx}	1.9921	2.0029
g_{yy}	2.0050	1.9997
g_{zz}	2.0018	2.0042
$A_{xx}(^{55}\text{Mn})/\text{MHz}$	+109.72	+109.68
$A_{yy}(^{55}\text{Mn})/\text{MHz}$	+109.03	+109.29
$A_{zz}(^{55}\text{Mn})/\text{MHz}$	+102.24	+102.79
$D^{\text{SS}+\text{SO}}/\text{cm}^{-1}$	+0.5578	+0.4933
$E^{\text{SS}+\text{SO}}/\text{cm}^{-1}$	-0.0298	-0.0868
$ E^{\text{SS}+\text{SO}}/D^{\text{SS}+\text{SO}} $	0.1663	0.1760

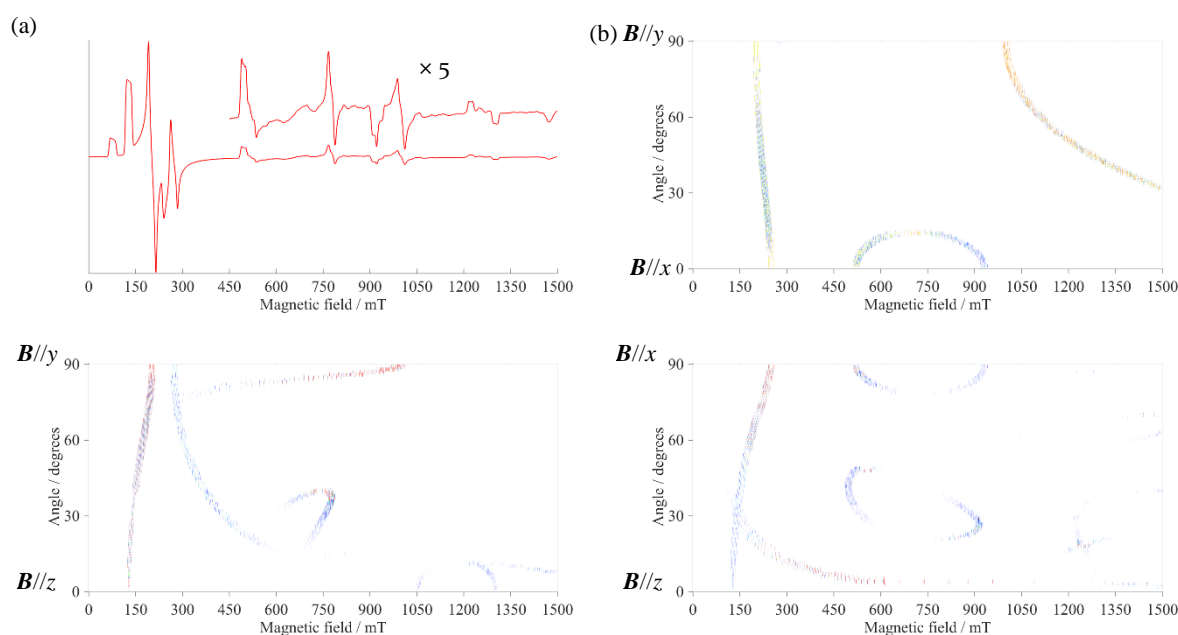


Fig. S6. (a) The theoretical X-band (9.45 GHz) ESR spectrum of **1** in powder at 90 K based on the full spin Hamiltonian which includes the rank-2 ZFS tensor. The spin Hamiltonian parameters are based on the theoretical ones, and the magnetic tensors are assumed to be collinear. (b) The angular dependence of the ESR spectra in only the three principal axis planes for clarity. The powder-pattern ESR spectra in (a) are obtained from the complete random orientations of the static magnetic field with the perpendicular microwave excitation. The principal values of theoretical magnetic parameters: $g_{xx} = 1.9921$, $g_{yy} = 2.0050$, $g_{zz} = 2.0018$, $A_{xx}(^{55}\text{Mn}) = 109.72$ MHz, $A_{yy}(^{55}\text{Mn}) = 109.03$ MHz, $A_{zz}(^{55}\text{Mn}) = 102.24$ MHz, $D^{\text{SS}+\text{SO}} = +0.5578$ cm^{-1} , $E^{\text{SS}+\text{SO}} = -0.0298$ cm^{-1} . The peak-to-peak linewidth for the single transition: 10 mT for (a) and 1 mT for (b). Colors denote the transition intensities.

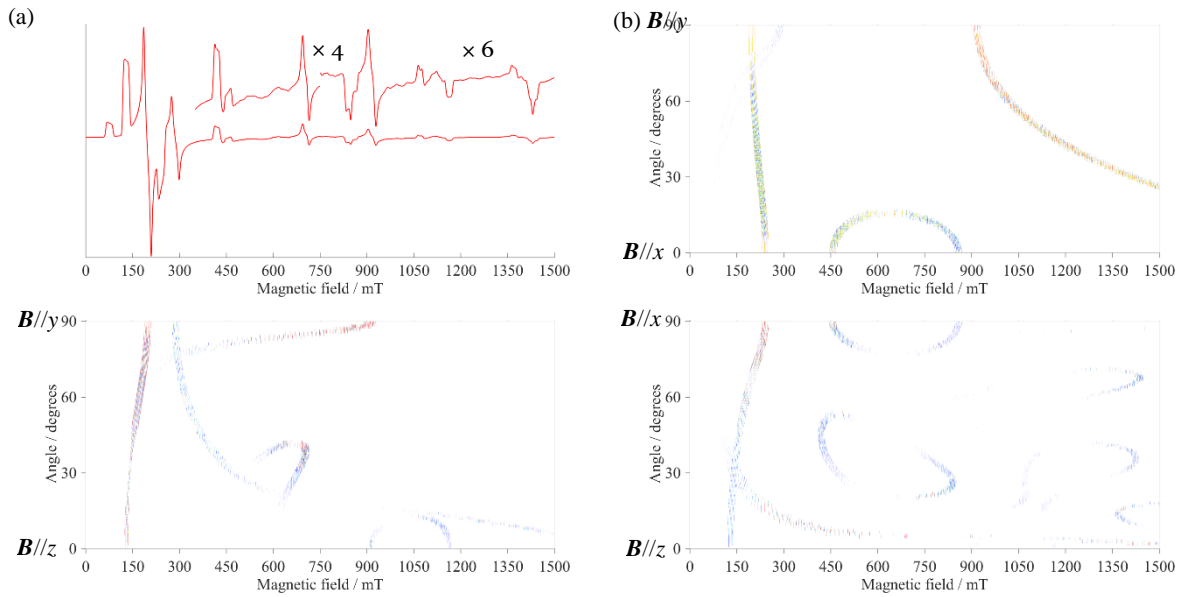


Fig. S7. (a) The theoretical X-band (9.45 GHz) ESR spectrum of **2** in powder at 90 K based on the full spin Hamiltonian which includes the rank-2 ZFS tensor. The spin Hamiltonian parameters are based on the theoretical ones, and the magnetic tensors are assumed to be collinear. (b) The angular dependence of the ESR spectra in only the three principal axis planes for clarity. The powder-pattern ESR spectra in (a) are obtained from the complete random orientations of the static magnetic field with the perpendicular microwave excitation. The principal values of theoretical magnetic parameters: $g_{xx} = 2.0029$, $g_{yy} = 1.9997$, $g_{zz} = 2.0042$, $A_{xx}({}^{55}\text{Mn}) = 109.68$ MHz, $A_{yy}({}^{55}\text{Mn}) = 109.29$ MHz, $A_{zz}({}^{55}\text{Mn}) = 102.79$ MHz, $D^{\text{SS}+\text{SO}} = +0.4933$ cm $^{-1}$, $E^{\text{SS}+\text{SO}} = -0.0868$ cm $^{-1}$. The peak-to-peak linewidth of 5 mT for (a) and 1 mT for (b). Colors denote the transition intensities.

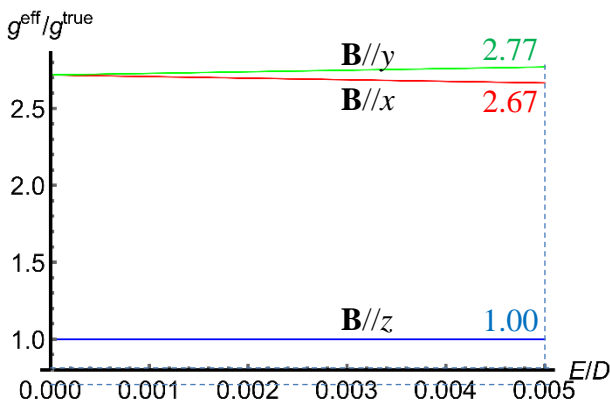


Fig. S8. The ratio of $g^{\text{eff}}/g^{\text{true}}$ as a function of E/D for the $|M_s = 1/2\rangle$ -dominant transition, as calculated by using the exact solution of the rank-2 ZFS + Zeeman interaction Hamiltonian for $h\nu/D = 9.45$ GHz/20 GHz = 0.47 with $S = 5/2$ in the case of the collinearity between the \mathbf{g} - and ZFS tensors (h denotes Planck constant and ν the microwave frequency). The $g^{\text{eff}}/g^{\text{true}}$ values at $E/D = 0.005$ are given for the x - and y -canonical orientations. [1]

(b) [FeTPP(4-PyNO)]BF₄ · 3 · BF₄: Complex 3

Table S4. The theoretical principal values and E/D of the magnetic tensors of complex 3^+ , as obtained by the quantum chemical calculations on the basis of the NOB-PK method at the UBP86/Sapporo-DZP, 3-21g level. The definition of the principal axes is given in the text. Importantly, the theoretical D -values are predicted to be positive. The ratios of the theoretical E/D values are overestimated, indicating that more rectified theoretical treatments of the magnetic tensors are required.

	3^+
g_{xx}	2.0099
g_{yy}	2.0095
g_{zz}	2.0092
D^{SS+SO}/cm^{-1}	+3.1241
E^{SS+SO}/cm^{-1}	-0.0830
$ E^{SS+SO}/D^{SS+SO} $	0.0266

Table S5. Comparison of the D^{SO} tensor contribution between the NOB-PK and PK Methods for complexes 1–3.

Molecule	NOB-PK-UBP86/Sapporo-DZP, 3-21g		PK-UBP86/Sapporo-DZP	
	D^{SO}/cm^{-1} *	E^{SO}/cm^{-1}	D^{SO}/cm^{-1}	E^{SO}/cm^{-1}
1	+0.5640	-0.0911	+2.0029 ^a	-0.5086
2	+0.5005	-0.0854	-0.9074 ^b	-0.0172
3⁺	+3.1056	-0.0801	+13.9192	+0.5111

*The $D^{SO}(\text{NOB-PK})_{zz}$ axis was perpendicular to the porphyrin plane.

^aThe $D^{SO}(\text{PK})_{zz}$ axis was nearly along the direction bisecting the angle between the $D^{SO}(\text{NOB-PK})_{xx}$ and $D^{SO}(\text{NOB-PK})_{yy}$ axes.

^bThe $D^{SO}(\text{PK})_{zz}$ axis was nearly parallel to the $D^{SO}(\text{NOB-PK})_{xx}$ axis.

Note that the D^{SO} -values obtained by the PK method are apart from the experimental ones (0.68 cm^{-1} for complex **1** (1-MeIm) and 0.67 cm^{-1} for complex **2** (2-MeHIm). The D^{SO} -value of complex 3^+ by the PK method is overestimated. On the other hand, the D^{SO} -values calculated by the NOB-PK method reasonably agree with the experimental ones.

Analysis of the SQUID Data of complex 3 revisited

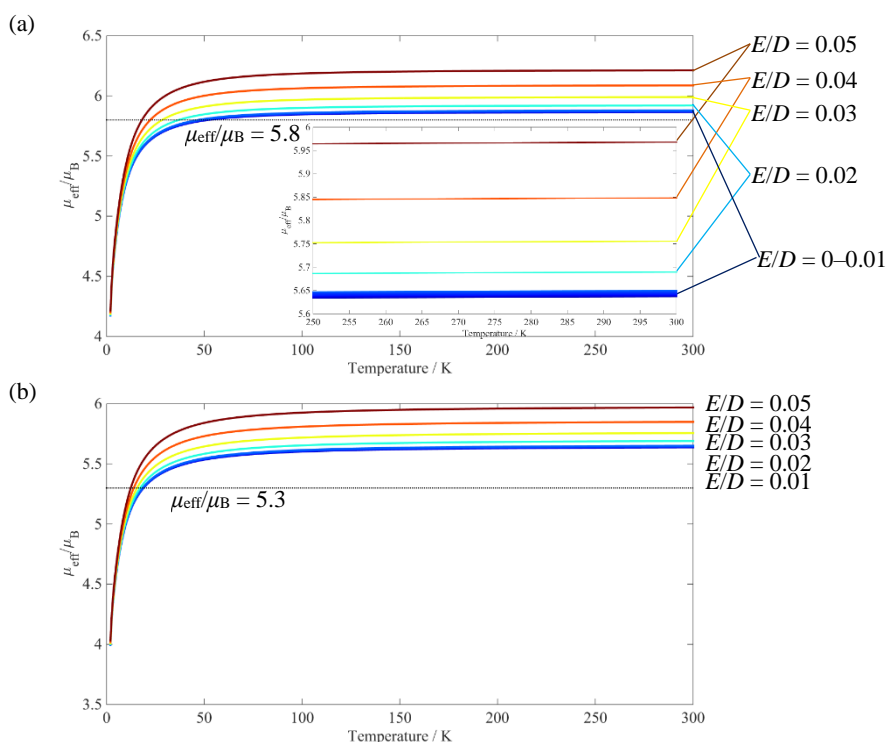


Fig. S9. The calculated temperature dependence of the effective magnetic moments (μ_{eff}) for (a) the solution and (b) micro-crystalline samples of $3 \cdot \text{BF}_4$. The ZFS + Zeeman interaction Hamiltonian was used with the true principal g -values converted from the fictitious spin-1/2 g -values ($g_{\perp}^{\text{eff}} = 5.94$, $g_{\parallel}^{\text{eff}} = 1.99$ for (a) and $g_{\perp}^{\text{eff}} = 5.62$, $g_{\parallel}^{\text{eff}} = 1.98$ for (b), respectively) by using of Eq. (4) in the text and the counterparts for the principal x - and y -axes. The D -value was estimated by reproducing the shape of the curves in the low temperature region. The dotted lines indicate the experimental values of the paramagnetic component at 300 K: $D = 300$ GHz with E/D in the range of 0 to 0.05. The detailed experimental data and procedure of the analysis were not given in the reported paper.

X-band (9.7 GHz)

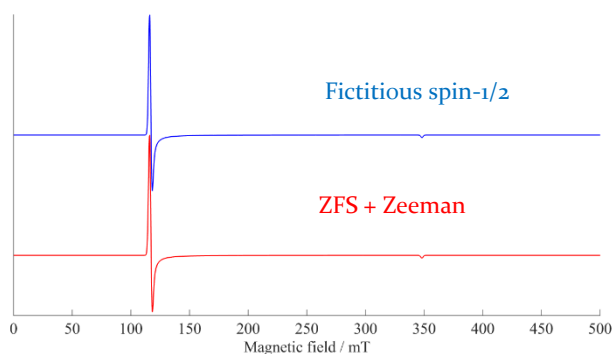


Fig. S10. The simulated spectrum of complex **3** based on the reported fictitious spin-1/2 magnetic tensors (blue) and the simulated one based on the ZFS + electronic Zeeman interaction Hamiltonian approach (red). The microwave frequency used was 9.7 GHz, the peak-to-peak line width for the single transition was 4.0 mT. The principal values of the magnetic tensors: $g_{\perp}^{\text{eff}} = 5.94$, $g_{\parallel}^{\text{eff}} = 1.99$ for the blue spectrum and $\mathbf{g}^{\text{true}} = [1.996 \ 1.965 \ 1.99]$, $D = +10 \text{ cm}^{-1}$ and $E/D = 0.001$ for the red one. The \mathbf{g} - and \mathbf{D} -tensors were collinear. Any strain effect of the tensor and the linewidth was not included. The simulated spectra were obtained by using EasySpin (ver. 5.1.12). [3]

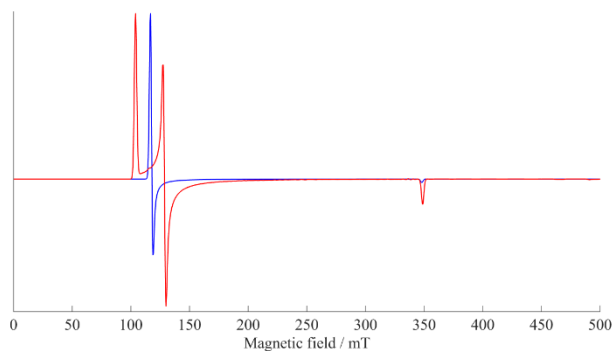


Fig. S11. The simulated spectrum of complex **3** based on the reported fictitious spin-1/2 magnetic tensors (blue) and the simulated one based on the theoretical magnetic tensors (red). The microwave frequency used was 9.7 GHz, and the peak-to-peak linewidth was 2.0 mT. The principal values of the magnetic tensors were $g_{\perp}^{\text{eff}} = 5.9$, $g_{\parallel}^{\text{eff}} = 2.0$ for the blue spectrum and $\mathbf{g}^{\text{true}} = [2.0099, 2.0095, 2.0092]$, $D = +3.1241 \text{ cm}^{-1}$ and $E = -0.0830 \text{ cm}^{-1}$ for the red spectrum. The red spectrum obviously shows that theory overestimates the asymmetry parameter $3E/D$. The \mathbf{g} - and \mathbf{D} -tensors were collinear. Any strain effect of the tensor and the linewidth was not included. The simulated spectra were obtained by using EasySpin (ver. 5.1.12). [3]

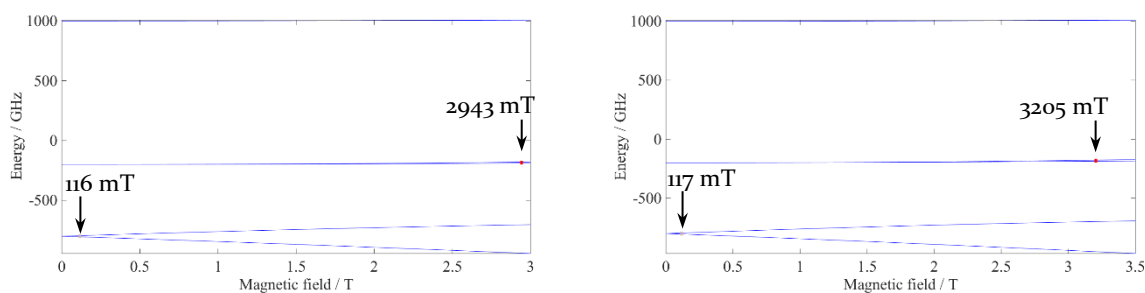


Fig. S12. The energy diagrams calculated for $\mathbf{3}^+$, ($S = 5/2$) in the case of the static magnetic field parallel to (a) the principal x -axis and (b) the principal y -axis (X-band). Magnetic tensors: $\mathbf{g}^{\text{true}} = [1.996, 1.965, 1.99]$, $D = 300 \text{ GHz}$ and $E/D = 0.001$. The \mathbf{g} - and \mathbf{D} -tensor were collinear. Microwave frequency used: 9.7 GHz. The diagrams were obtained using EasySpin (ver. 5.1.12). [3] The calculated resonance fields are 116 mT and 2943 mT for $\mathbf{B} // x$ and 117 mT and 3205 mT for $\mathbf{B} // y$.

Q-band (33 GHz)

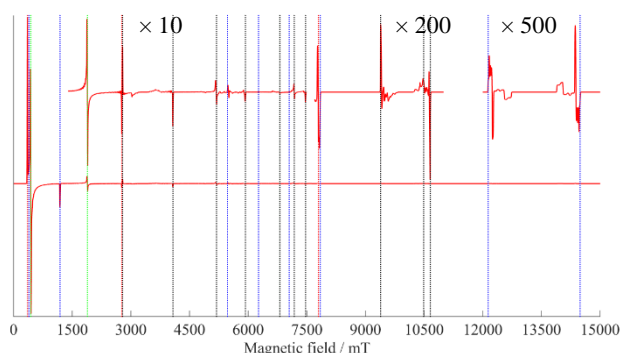
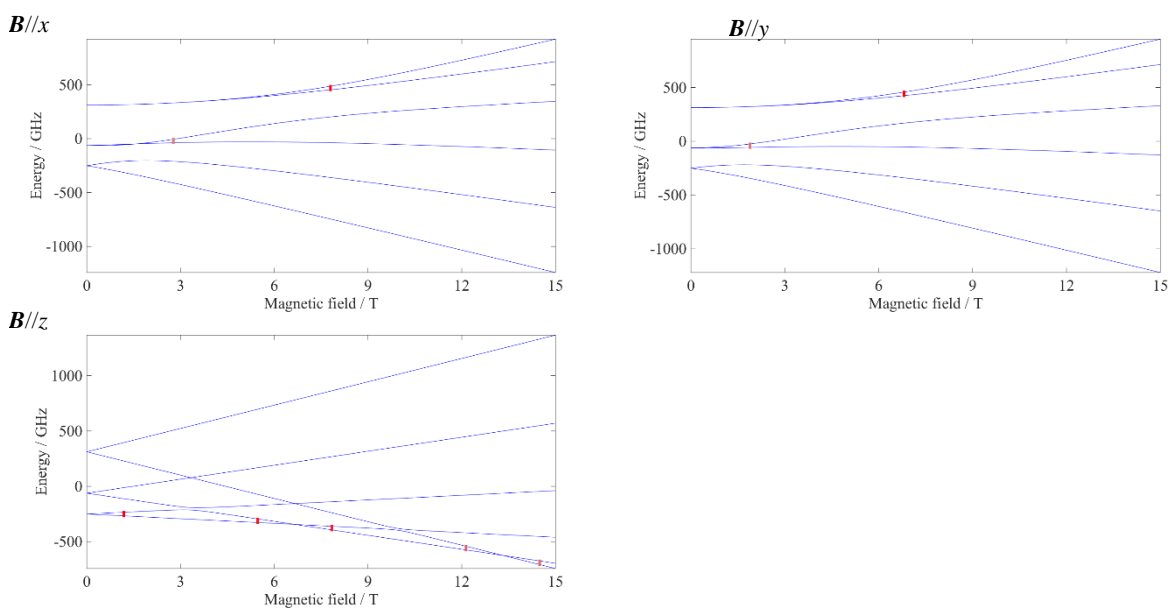


Fig. S13. The simulated Q-band ESR spectrum of complex 3^+ based on the reported magnetic tensors (spectrum in blue) and the theoretical magnetic tensors (spectrum in red). The microwave frequency used was 33 GHz, and the peak-to-peak linewidth was 10.0 mT. The principal values of the magnetic tensors were $g_{\perp}^{\text{eff}} = 5.9$, $g_{\parallel}^{\text{eff}} = 2.0$ for the blue spectrum and $g^{\text{true}} = [2.0099, 2.0095, 2.0092]$, $D = +3.1241 \text{ cm}^{-1}$ and $E = -0.0830 \text{ cm}^{-1}$ for the red spectrum. The g - and D -tensors were collinear. Any strain effect of the tensor and the linewidth was not included. The simulated spectra were obtained by using EasySpin (ver. 5.1.12). [3] The vertical dotted lines denote the resonance positions of the principal axis canonical and off-principal axis extra peaks.



x -axis: 356.3 mT, 2770 mT, 7800 mT

y -axis: 442.0 mT, 1888 mT, 6808 mT

z -axis: 392.8 mT, 1190 mT, 5471 mT, 6266 mT, 7051 mT, 7843 mT, 12140 mT, 14490 mT

off-axis: 2788 mT, 4078 mT, 5190 mT, 5931 mT, 6810 mT, 7179 mT, 7468 mT, 9391 mT, 10660 mT

Fig. S14. The energy diagrams calculated for 3^+ , ($S = 5/2$) in the case of the static magnetic field parallel to (a) the principal x -axis and (b) the principal y -axis (Q-band). Magnetic tensors: $g^{\text{true}} = [2.0099, 2.0095, 2.0092]$, $D = +3.1241 \text{ cm}^{-1}$ and $E = -0.0830 \text{ cm}^{-1}$. The g - and D -tensor were collinear. Microwave frequency used: 33 GHz. The diagrams were obtained using EasySpin (ver. 5.1.12). [3]

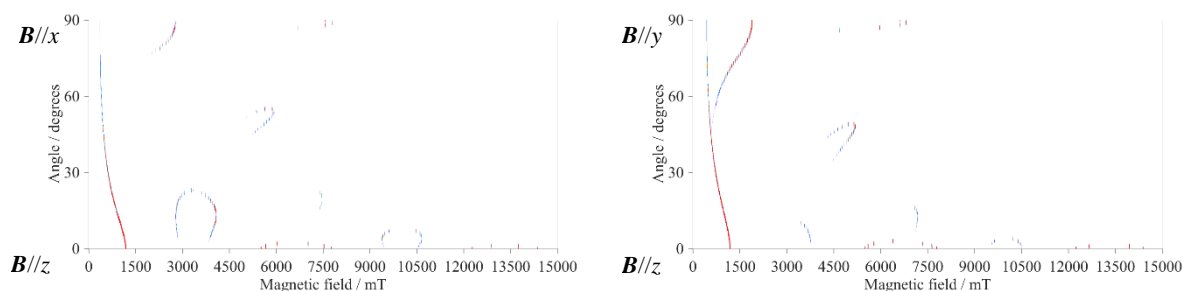


Fig. S15. The simulated angular dependence of ESR spectra of 3^+ by using of the calculated magnetic parameters: $\mathbf{g}^{\text{true}} = [2.0099, 2.0095, 2.0092]$, $D = +3.1241 \text{ cm}^{-1}$ and $E = -0.0830 \text{ cm}^{-1}$ with a peak-to-peak linewidth of 1 mT for. Microwave frequency used: 33 GHz. The simulated spectra were obtained using EasySpin (ver. 5.1.12) [3] with varying the angle of the magnetic field one-degree stepwise.

W-band (95 GHz)

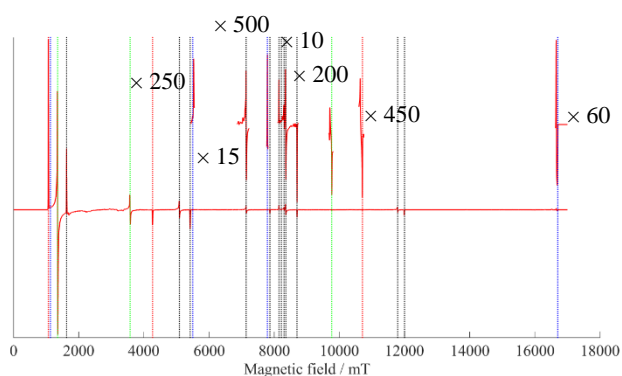
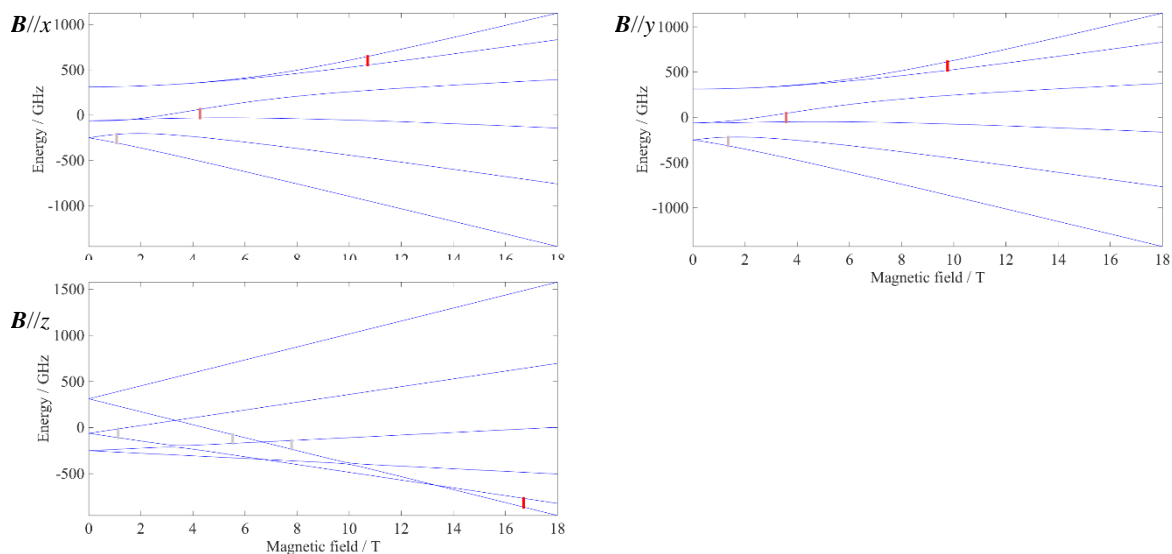


Fig. S16. The simulated W-band ESR spectrum of 3^+ based on the reported magnetic tensors and the theoretical magnetic tensors. The microwave frequency used was 95 GHz, and the peak-to-peak line width was 10.0 mT. The principal values of the magnetic tensors were $\mathbf{g}^{\text{true}} = [2.0099, 2.0095, 2.0092]$, $D = +3.1241 \text{ cm}^{-1}$ and $E = -0.0830 \text{ cm}^{-1}$ for the red one. The \mathbf{g} - and \mathbf{D} -tensors are collinear. Any strain effect of the tensor and the linewidth was not included. The simulated spectra were obtained by using EasySpin (ver. 5.1.12). [3] The vertical dotted lines denote the resonance positions of the principal axis canonical and off-principal axis extra peaks.



x -axis: 1071 mT, 4270 mT, 10710 mT

y -axis: 1353 mT, 3578 mT, 9763 mT

z -axis: 1131 mT, 5500 mT, 7788 mT, 16700 mT

off-axis: 5090 mT, 5420 mT, 7140 mT, 7870 mT, 8150 mT, 8220 mT, 8300 mT, 8360 mT, 8700 mT, 11790 mT, 12000 mT

Fig. S17. The energy diagrams of 3^+ calculated with the static magnetic field oriented parallel to the principal axes. The theoretical magnetic tensors used: $\mathbf{g}^{\text{true}} = [2.0099, 2.0095, 2.0092]$, $D = +3.1241 \text{ cm}^{-1}$ and $E = -0.0830 \text{ cm}^{-1}$. Microwave frequency: 95 GHz.

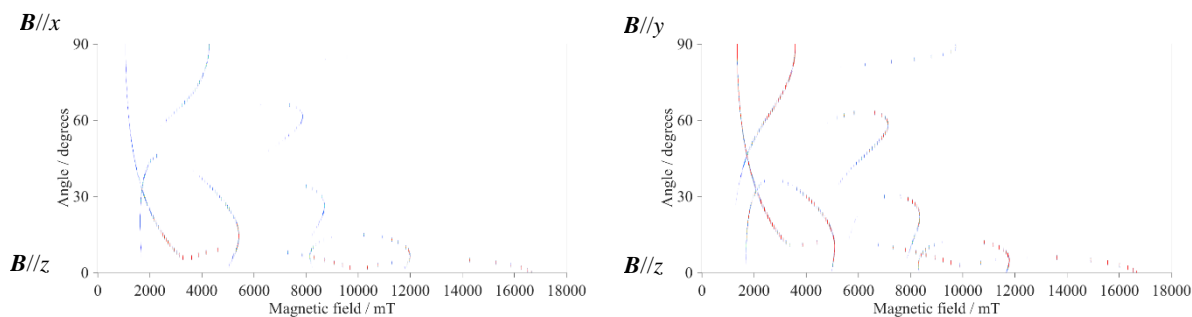


Fig. S18. The simulated angular dependence of ESR spectra of 3^+ by using of the calculated magnetic parameters: $\mathbf{g}^{\text{true}} = [2.0099, 2.0095, 2.0092]$, $D = +3.1241 \text{ cm}^{-1}$ and $E = -0.0830 \text{ cm}^{-1}$ with a peak-to-peak linewidth of 1 mT for. Microwave frequency used: 95 GHz. The simulated spectra were obtained using EasySpin (ver. 5.1.12) [3] with varying the angle of the magnetic field one-degree stepwise.

(c) $cis\text{-}[\text{Co}^{\text{II}}(\text{hfac})_2(\text{H}_2\text{O})_2]$, complex 4

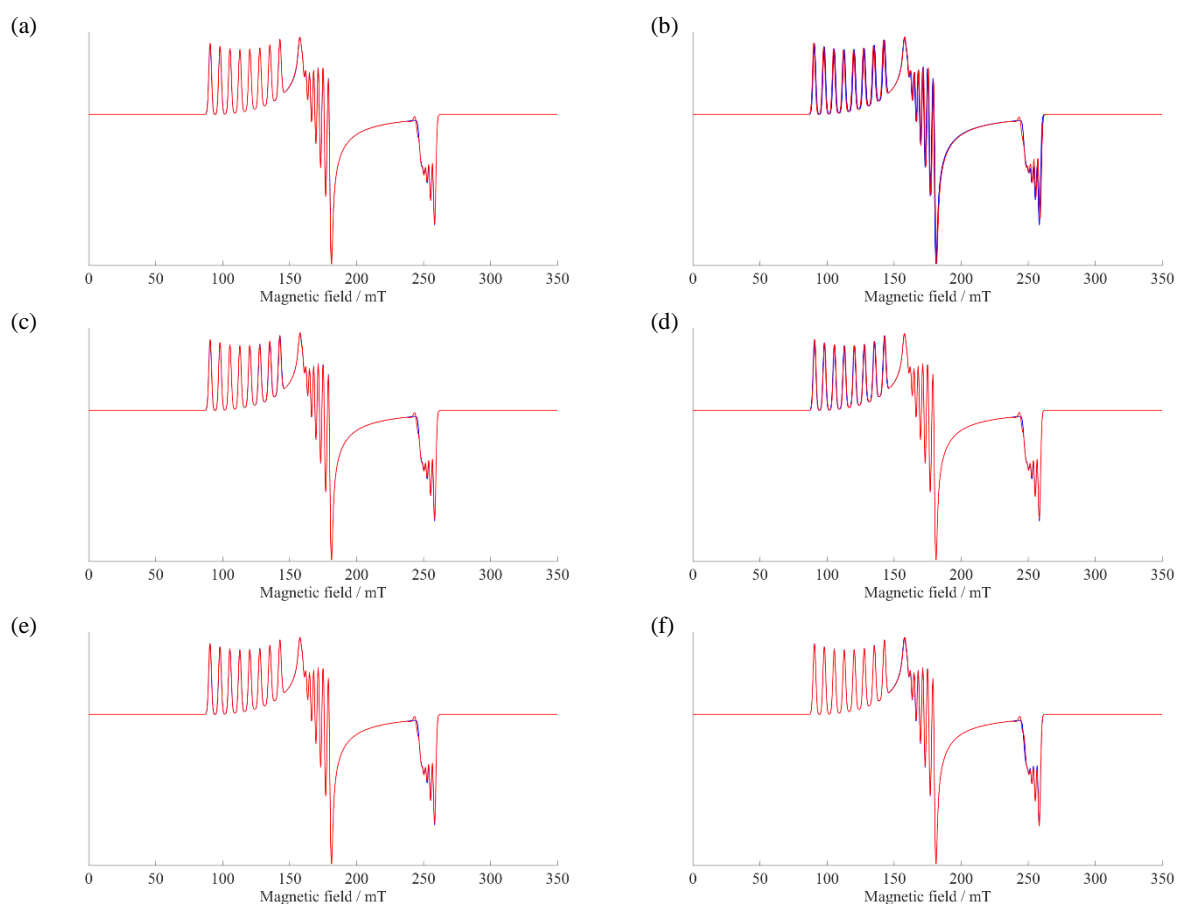


Fig. S19. The ESR spectra of complex 4 obtained from the fictitious spin-1/2 and full spin Hamiltonians with (a) $E/D =$ (a) 0.05, (b) 0.1, (c) 0.15, (d) 0.2 (e) 0.25 and (f) 0.3. The optimized true principal g -values are summarized in Table S6 below. The peak-to-peak linewidth was 2 mT. The g - and ZFS tensors were assumed to be collinear.

Table S6. The sets of spin Hamiltonian parameters obtained from the spectral simulation. The g -values are given as optimized as a function of E/D .

	$B // x$	$B // y$	$B // z$
g^{eff} (ref. 4)	3.98	5.79	2.67
g^{true}			
$E/D = +0.05$	2.698	2.156	2.6915
+0.1	2.550	2.350	2.750
+0.15	2.410	2.597	2.855
+0.2	2.300	2.888	3.002
+0.25	2.223	3.237	3.198
+0.3	2.156	3.654	3.445

The true principal g -tensors based on the full spin Hamiltonian (1) were optimized for the fixed E/D values (0.05, 0.1, 0.15, 0.2, 0.25 and 0.3).

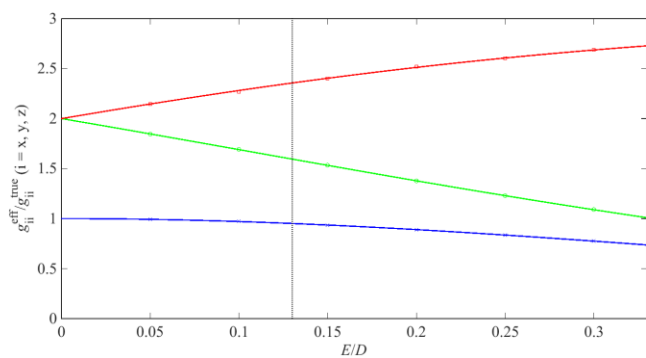


Fig. S20. The plot of $g^{\text{eff}}/g^{\text{true}}$ shown in Table S6. The red, green and blue lines were calculated by using Eqs. (3a)–(3c) for the $|M_S = \pm 1/2\rangle$ dominant transitions corresponding to the principal x -, y - and z -axes, respectively. [1] A vertical dotted line is at $E/D = 0.13$.

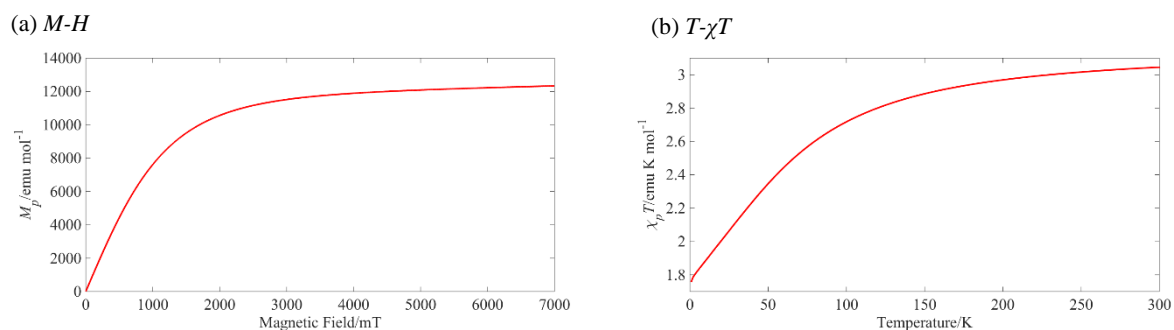


Fig. S21. The simulated (a) magnetization curve and (b) magnetic susceptibility of complex 4. Both the rank-2 ZFS and the electronic-Zeeman interaction tensors were considered in the spin Hamiltonian.

Non-collinear case

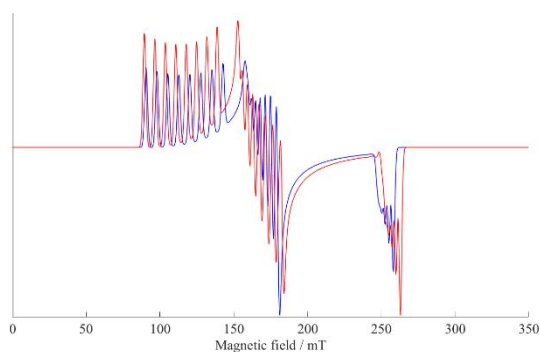


Fig. S22. The simulated randomly-oriented (powder-pattern) ESR spectra of **4** magnetically diluted in diamagnetic *cis*-[Zn(hfac)₂(H₂O)₂]. The spectra in blue and red are based on the fictitious spin-1/2 and ZFS/e-Zeeman spin Hamiltonian approach, respectively. Microwave frequency used: 9.4715 GHz, peak-to-peak linewidth: 2.0 mT. Magnetic tensors: $g^{\text{eff}} = [5.79, 2.67, 3.98]$, $A^{\text{eff}}(^{59}\text{Co}) = [603.6, 58.82, 167.63]$ MHz and $g^{\text{true}} = [2.7, 2.75, 2.25]$, $A^{\text{true}}(^{59}\text{Co}) = [99.2, 264.6, 61.0]$ MHz, $D = 2.0 \times 10^3$ GHz and $E/D = 0.10$. The **A**- and **D**-tensors were assumed to be collinear, while the **g**-tensor was rotated 0, 90 and 138 degrees (in Euler angles) with respect to the **D**-tensor. Any strain effect of the tensor and the linewidth was not included. The simulated spectra were obtained by using EasySpin (ver. 5.1.12). [3]

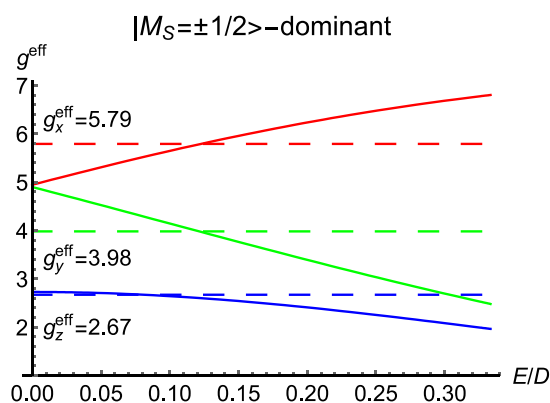


Fig. S23. The relationships of the g^{eff} and g^{true} -values calculated with the exact eigenenergies in the non-collinear case. The solid curves were the calculated effective g -values from the true g -values ($g_x = 2.7$, $g_y = 2.75$ and $g_z = 2.25$) as a function of E/D for each axis. The E/D ratio used in the simulated spectrum (red line in Fig. 5) was obtained as the crossing point between the solid and the dashed lines. The g_x^{eff} and g_y^{eff} curves give $E/D = 0.12$ for the crossing points, and the g_z^{eff} one $E/D = 0.10$. Note that the experimental error for the ratio of E/D was estimated to be ± 0.02 . The experimental effective g -values (5.79, 3.98 and 2.67) denoted by the dashed lines were reported in ref. [4].

References

- [1] T. Yamane, K. Sugisaki, T. Nakagawa, H. Matsuoka, T. Nishio, S. Kinjyo, N. Mori, S. Yokoyama, C. Kawashima, N. Yokokura, K. Sato, Y. Kanzaki, D. Shiomi, K. Toyota, D. H. Dolphin, W.-C. Lin, C. A. McDowell, M. Tadokoro and T. Takui, Analyses of Sizable ZFS and Magnetic Tensors of High Spin Metallocomplexes, *Phys. Chem. Chem. Phys.*, 2017, **19**, 24769–24791.
- [2] Q. Yu, Y. Liu, D. Liua and J. Li, Geometric and Electronic Structures of Five-Coordinate Manganese(II) “Picket Fence” Porphyrin Complexes, *Dalton Trans.*, 2015, **44**, 9382–9390.
- [3] S. Stoll and A. Schweiger, EasySpin, a Comprehensive Software Package for Spectral Simulation and Analysis in EPR, *J. Magn. Reson.*, 2006, **178**, 42–55.
- [4] D. V. Korchagin, A. V. Palii, E. A. Yureva, A. V. Akimov, E. Ya. Misochko, G. V. Shilov, A. D. Talantsev, R. B. Morgunov, A. A. Shakin, S. M. Aldoshin and B. S. Tsukerblat, Evidence of Field Induced Slow Magnetic Relaxation in *cis*-[Co(hfac)₂(H₂O)₂] Exhibiting Tri-Axial Anisotropy with a Negative Axial Component, *Dalton Trans.*, 2017, **46**, 7540–7548.